Elements of Photonics, Volume II: For Fiber and Integrated Optics. Keigo Iizuka

ISBNs: 0-471-40815-8 (Hardback); 0-471-22137-6 (Electronic)

12

DETECTING LIGHT

This chapter begins with a description of light detectors used in optics laboratories (Sections 12.1 through 12.3). Then, special purpose detectors used primarily for optical communication systems are described. These include the PIN photodiode and APD detectors (presented in Section 12.4).

The remaining sections deal with various methods of detection employed in fiber-optic communication systems. Direct detection is a simple method that measures only the intensity of light, and this method is described in Section 12.5. Sections 12.6 to 12.8 are devoted to coherent detection, which can measure not only the intensity but also the phase and frequency of the light. Lastly, Section 12.9 looks at phase and polarization jitters.

The signal to noise ratio (S/N) of the detection system will be presented in connection with optical communication systems in Chapter 16.

12.1 PHOTOMULTIPLIER TUBE

Light detectors convert light energy into an electrical signal. The photomultiplier tube (PMT) has an ultrahigh sensitivity and is widely used in optics research laboratories. The sensitivity is so high that it can almost detect a single photon.

Figure 12.1 explains the structure of the photomultiplier tube. The photomultiplier tube is a combination of the cathode, which is the photon–electron converter, and the dynodes, which act as amplifiers of the converted electrons.

The photoelectric converter section consists of the cathode and the first dynode. The cathode surface is coated with a low-work-function material, such as alkali metals. When the incident photons bombard the cathode, electrons are ejected from the surface. Emission, however, takes place only when a quantum $h\nu$ of the incident light is larger than the work function ϕ of the cathode material:

$$\phi < h\nu \tag{12.1}$$

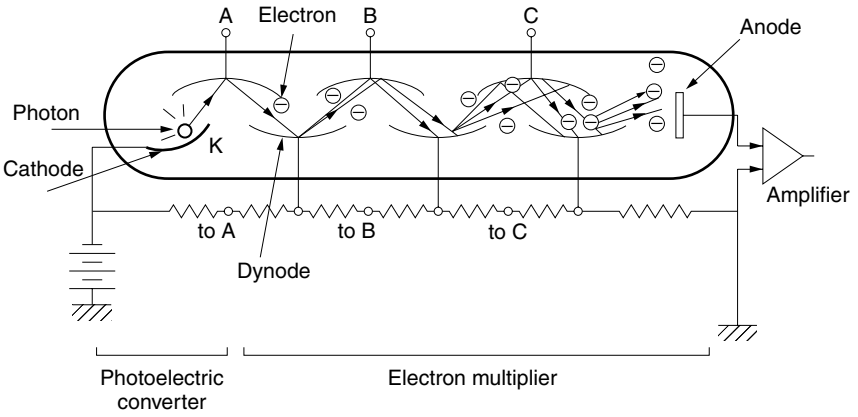

Figure 12.1 Photomultiplier tube. Points A, B, C ... at the bottom are connected, respectively, to the A, B, C, ... dynodes at the top.

where h is Planck's constant 6.63×10^{-34} J · s. Thus, the coating material of the cathode determines the range of wavelength for usable light. A number of materials are available in the visible wavelength range but, unfortunately, high-sensitivity materials have not been found in the infrared region, where the optical communication system operates.

The electrons ejected from the cathode are accelerated by the high voltage between the cathode and the first dynode and then strike the surface of the dynode with high energy. Secondary electrons are emitted from the dynode in larger numbers. With a series of dynodes operating at gradually higher voltages, the number of secondary electrons are multiplied at each dynode. The multiplied secondary electrons are collected by the anode whose potential is typically a few kilovolts higher than the cathode.

Next, the sensitivity of the photomultiplier tube will be calculated. Let W be the energy of the light entering the cathode of the photomultiplier tube. The number of photons in terms of the incident light energy is $W/h\nu$.

Let η be the quantum efficiency, which is defined as the ratio of the number of generated electrons to incident photons. Each electron carries charge e. The total amount of charge Q accumulated at the cathode is

$$Q = \eta \frac{e}{h\nu} W \tag{12.2}$$

The current from the cathode is obtained by taking derivatives of both sides of Eq. (12.2),

$$i_{\text{cathode}} = \eta \frac{e}{h\nu} P \tag{12.3}$$

where P is the incident light power.

If in each dynode stage one electron generates δ secondary electrons, the total multiplication M from the N dynodes is

$$M = \delta^N \tag{12.4}$$

Thus, the output current from the photomultiplier tube is

$$i = \eta \frac{e}{h\nu} MP \tag{12.5}$$

Finally, the responsivity R of the photomultiplier tube, which is the output current with unit incident light power, is

$$R = \eta \frac{e}{h\nu} M \text{ A/W} \tag{12.6}$$

where A/W is amperes/watt. The responsivity is used to characterize a photomultiplier tube.

Typical values are inserted into Eq. (12.6) to calculate the responsivity of the photomultiplier.

$\eta = 0.01$
$\lambda = 0.63$ μm or $\nu = 4.76 \times 10^{14}$ Hz
$\delta = 5$
$N = 10$

$$R = 0.01 \frac{(1.6 \times 10^{-19})(5^{10})}{(6.63 \times 10^{-34})(4.76 \times 10^{14})}$$
$$\div 5 \times 10^4 \text{ A/W}$$

The responsivity of a PIN photodiode is typically $R = 0.5$ A/W and the photomultiplier tube is significantly more sensitive.

The internal impedance of a photomultiplier being as high as 10 MΩ, the matched load impedance can be selected high so that a high output voltage can be achieved. For instance, for 1 pW (−90 dBm) of input light, the output voltage across the 10-MΩ load resistance R_L is

$$V_{\text{out}} = RPR_L = (5 \times 10^4)(10^{-12})(10^7) = 0.5 \text{ V}$$

It should, however, be remembered that such a large load resistance raises the value of the time constant CR_L of the detector, where C is the capacitance of the tube, and the response time of the tube becomes excessively slow.

Despite the high sensitivity of the photomultiplier tube, it is not practical for use as a detector for optical communication systems. These systems operate in the $\lambda = 1.3$ or 1.55 μm regions where the photomultiplier sensitivity is low. Other disadvantages of the photomultiplier tube when used for optical communication systems are poor frequency response, large size, the necessity of a kilovolt power supply, the limited lifetime of the tube, and the cost.

12.2 STREAK CAMERA

A streak camera is used to observe light variations with respect to time of the order of picoseconds (10^{-12} s). The structure of the streak camera, which is shown in Fig. 12.2a,

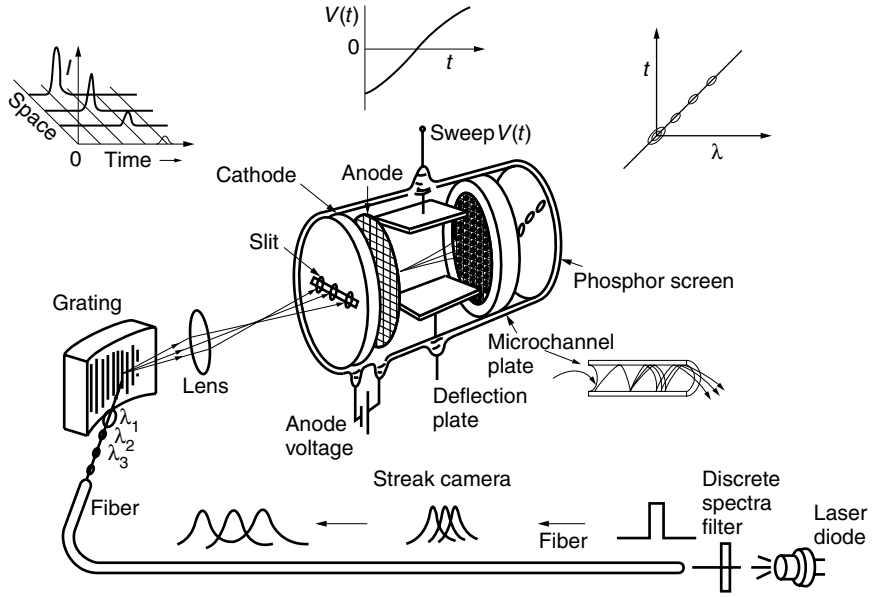

(a)

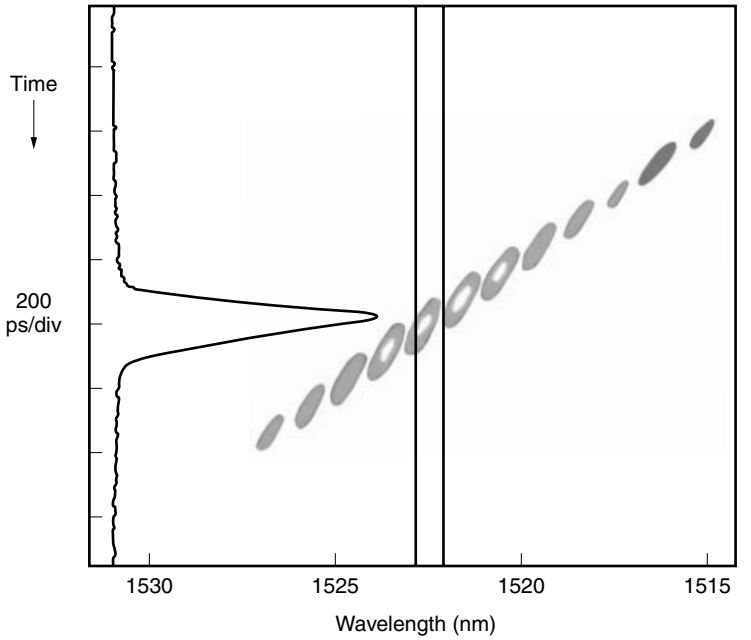

(b)

Figure 12.2 Streak camera measuring (a) the dispersion during transmission in an optical fiber and (b) chromatic dispersion in single-mode optical fiber. (After Y. Tsuchiya [1].)

is quite similar to a cathode ray tube used for an oscilloscope. The major difference is that the cathode ray tube uses a steady electron beam supplied by an electron gun installed in the tube, while the streak camera uses the electrons that are generated by the bombardment of incident photons onto a low-work-function cathode and formulated as a beam by the anode.

Another feature is that even though the location of the electron gun of the cathode ray tube is fixed, the photocathode of the streak camera is sensitive along the horizontal slit, and the location of the incident light is another piece of information that the streak camera can supply. Thus, the streak camera provides simultaneously three kinds of information: the intensity of the light, the time of arrival, and the location of the incidence.

For higher speed operation the sawtooth deflector voltage is sometimes replaced by a high-frequency sinusoidal voltage.

The variation of the incident light intensity is observed as a function of time on the fluorescent screen. In order to enhance the electron density hitting the fluorescent screen, a microchannel plate is installed between the deflector plate and the fluorescent screen. The microchannel plate is made up of a honeycomb of fine dynode tubes. As the wall bounces the electron beam, the electron beam is intensified.

Figure 12.2a shows an example of using the streak camera to measure the dispersion phenomenon in an optical fiber. A pulse having different wavelengths is launched simultaneously into a long optical fiber. The difference in arrival time of the different wavelength components is measured by the streak camera. The light components arriving at a later time see a higher deflector voltage $V(t)$ and are deflected higher. A display such as the one shown in Fig. 12.2b is obtained [1].

12.3 MISCELLANEOUS TYPES OF LIGHT DETECTORS

Other types of light detectors [2–4] are summarized here. When light illuminates such materials as CdS or CdSe, the surface conductivity increases due to the photoconductive effect. The device based on this phenomenon is known as the *photoconductor cell* or *photocell*. A special feature of the CdS photocell is that its spectral response characteristics resemble that of the human eye. It is widely used as an exposure meter in photography.

Solar cells convert solar energy into electrical energy by a phenomenon known as the *photovoltaic effect*. Calibrated solar cells are also used as light meters for photography.

The phototransistor is the amalgamation of a photodiode, which will be explained extensively in the next section, and an amplifier transistor. It is like a photomultiplier tube made of semiconductor material. It can provide a large signal output, but the response time is not as high as the photodiode alone.

Calorimetric methods use the temperature rise in a heat-absorbing strip that is exposed to light. The temperature rise is measured by a thermometer with as low a heat capacity as possible. These thermometers include a thermocouple, which establishes the voltage due to the temperature difference between the ambient and the heat-absorbing strip, and a thermister or bolometer, which changes its resistance in accordance with its temperature.

As an example of a device based on the calorimetric method, Fig. 12.3 shows a diagram of a pyrometer that measures the temperature distribution inside a furnance

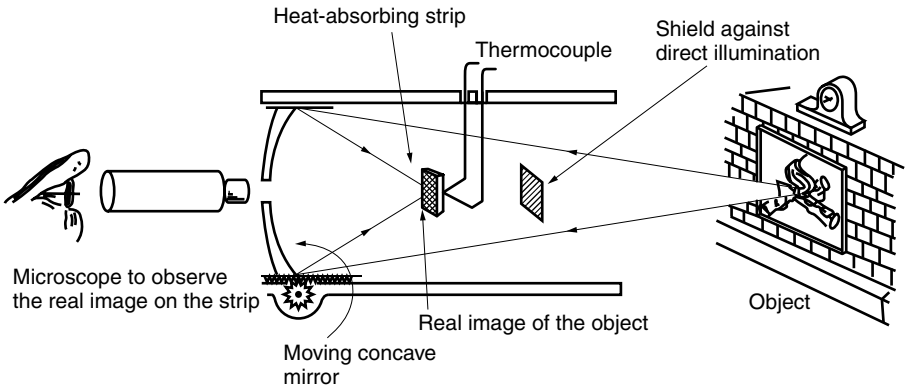

Figure 12.3 Pyrometer structure.

by measuring the radiating light intensity. The position of the concave mirror is adjustable so that the real image of the desired point of the radiation is focused onto the heat-absorbing strip. The attached microscope is used to observe the real image. The temperature rise of the strip is measured by a thermocouple. The measured intensity of light correlates with the temperature of the desired point in the furnace.

None of the devices in this section are suitable for fiber-optic communication because of the relatively slow response time. Detectors for fiber-optic communication are presented in the next section.

12.4 PIN PHOTODIODE AND APD

The basic principles of the PIN photodiode (PIN diode) and avalanche photodiode (APD) are quite similar to each other. Once the fundamental principles have been established for the PIN photodiode, the transition to understanding the avalanche photodiode will be quite easy.

Figure 12.4 shows the basic structure of the PIN and APD photodetectors. Basically, a PIN photodiode consists of three layers of semiconductor material: the p-type, the intrinsic-type, and the n-type semiconductors.

The actual physical structures of the PN and PIN photodetectors and the APD are presented in the next section; the PN and PIN photodetectors and the APD on an atomic scale are described in Appendix A of Volume II.

12.4.1 Physical Structures of PIN and APD Photodetectors

Figure 12.5a shows typical physical structures for the PIN and PN photodetectors [4,5]. There is very little difference between PN and PIN diodes. A PN diode is a diode formed by joining a p layer directly to an n layer, whereas a PIN diode is formed by joining a p layer to an intrinsic layer and then to an n layer. The p^+-type window layer is made extremely thin ($\sim$0.3 μm) because the light is incident from this layer and any charge carriers (electrons and holes) produced in the p^+ layer are subjected to a low electric field because of the high conductivity of the heavily doped p^+ layer. The lower electric field means slower response time and adds to the noise.

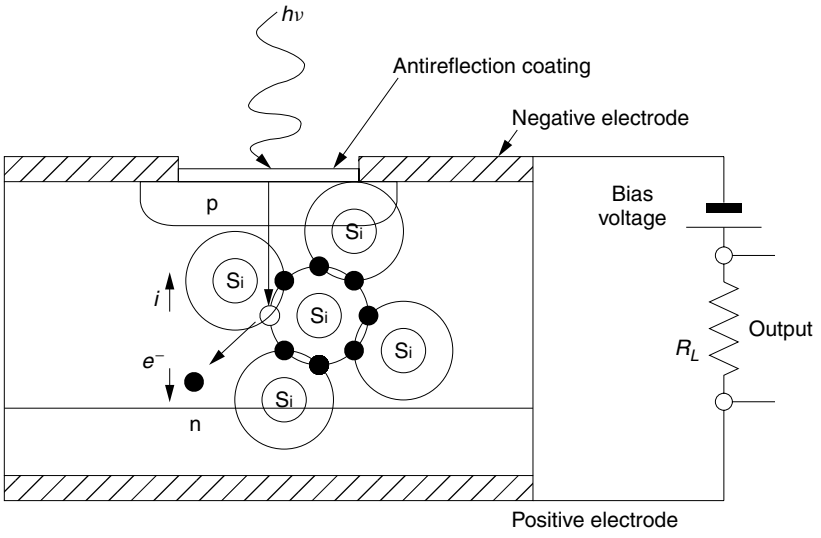

Figure 12.4 Basic structures of PN, PIN, and APD photodetectors.

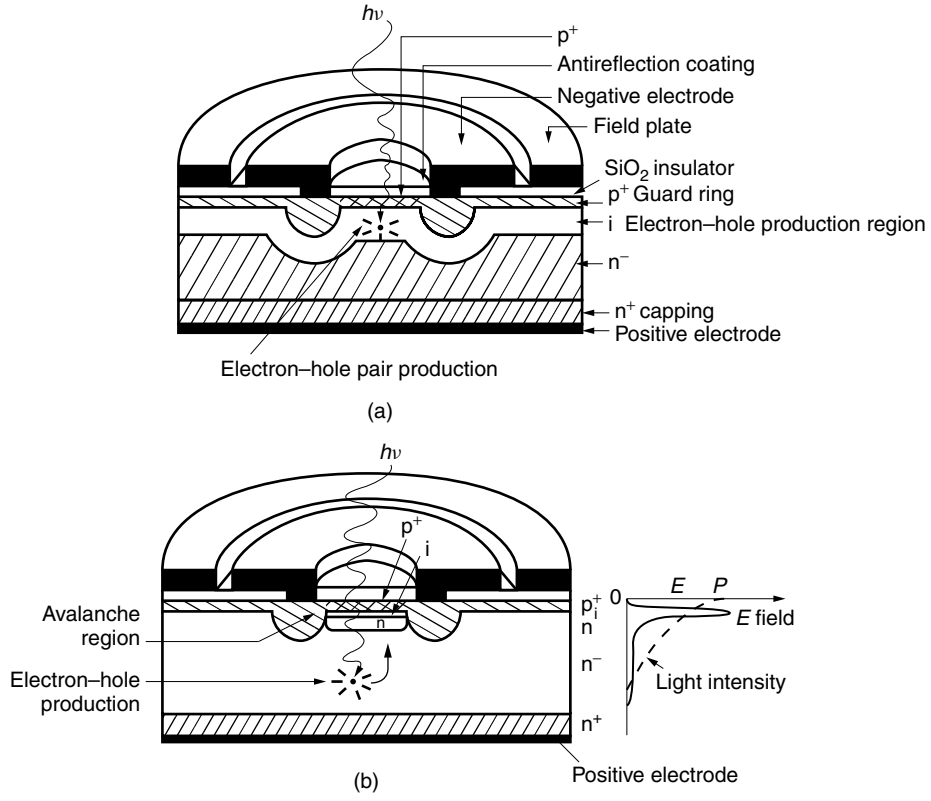

Figure 12.5 Structure of photodetectors. (a) PN and PIN photodiodes. (b) Avalanche photodiode (APD).

The light aperture is usually circular (Fig. 12.5 shows the cross section in a plane perpendicular to that of the circular aperture). A circular electrode is deposited over an insulating layer of SiO_2 and the p^+ layer guard ring. The purpose of the guard ring is to prevent dielectric breakdown by spreading the electric lines of force from the edge of the electrode. An antireflection (AR) coating is deposited over the aperture to minimize the amount of incident light that is reflected. Compared to a PN diode, the PIN diode has a thicker (a few μm thick) intrinsic layer that increases the interaction region for the incident photons with orbital electrons. An excessively long intrinsic region, however, harms the response time because the transit time for the electrons to reach the electrodes becomes too long. The diameter of the electrode is made small to minimize the capacitance. A metal field plate is deposited in order to prevent stray light entering the diode.

On the bottom side of the substrate, a highly doped n^+ capping layer is deposited to ensure better adhesion to the electrode in order to minimize the series resistance.

Figure 12.5b shows the structure of the avalanche photodiode [4] (APD). An APD has additional regions for accelerating the drift velocity of the carriers and multiplying the number of carriers by the avalanche effect. The bottom structure of the APD is identical with that of the PIN photodiode. The top p-i-n layers are multiplier layers. The resistivity of the i-type layer is made much higher than the other layers so that the potential drop across all the layers in series is concentrated in this layer.

Incident light is first converted into electric charge carriers in the n^- region. The generated carriers drift upward into the n-type layer because of the moderate electric field. The carriers then enter the highly resistive i-type layer. This i-type layer is not a separately deposited layer. Rather, it is the depletion region formed when the p^+ layer is joined to the n layer. Because of the combination of high resistivity and thinness, the field intensity in the i layer is so large that the collisions of the accelerated electrons with the crystal lattice result in the creation of new carriers. The electric field intensity reaches as high as 10^5 V/cm or even higher (the breakdown voltage of air is 3×10^4 V/cm), which is necessary to start the avalanche effect. The new carriers are also accelerated and collide with the crystal lattice in the avalanche region and generate even more carriers. The density of carriers multiplies as this snowball effect is triggered. Finally, the charge carriers exit from the top electrodes.

Thus, the bottom half of the APD has the function of converting the incident photons into electrons, and the top half has the function of amplifying the number of electrons generated. The APD performs the dual functions of photoelectric conversion and electric amplification.

12.4.2 Responsivity of the PIN Photodiode and APD

Expressions will be derived for the output current from a PIN photodiode and APD due to the incident light. The expressions are quite similar to those of a photomultiplier. Let W be the energy of the light entering the detector. The number of incident photons expressed in terms of the incident light energy is $W/h\nu$. Let η be the quantum efficiency, which is defined as the ratio of the number of generated electrons to incident photons. Each electron carries a charge e and the total amount of charge Q after multiplication due to the avalanche effect is

$$Q = \eta \frac{e}{h\nu} MW \tag{12.7}$$

M is the multiplication factor due to the avalanche effect. The derivative of Eq. (12.7) with respect to time gives the output current from the diode

$$i_s = \eta \frac{e}{h\nu} M P_s \quad \text{or} \quad i_s = \eta \frac{e\lambda}{hc} M P_s \tag{12.8}$$

where P_s is the incident light power.

It should be noted that the above definition of η includes (1) the finite transmission of light into the surface with transmission coefficient Eq. (2.16), (2) the exponential decay of the light power inside the intrinsic region, and (3) the finite length of the intrinsic region for generating electron-hole pair production over and above the probabilistic nature of electron-hole pair production.

Equation (12.8) indicates that the output current increases linearly with the wavelength of the incident light. There is, however, an upper limit on the wavelength. For the photon to ionize the atoms in the crystal lattice, the energy quantum $h\nu$ of the incident photon has to be larger than the bandgap energy E_g of the semiconductor. The quantum efficiency η has a rather abrupt cutoff wavelength in the longer wavelength region, as shown in Fig. 12.6a. In practice, the quantum efficiency decreases faster

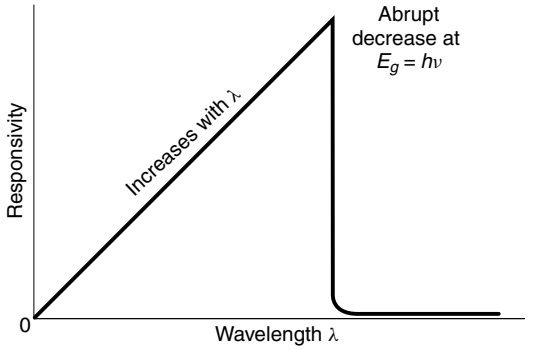

(a)

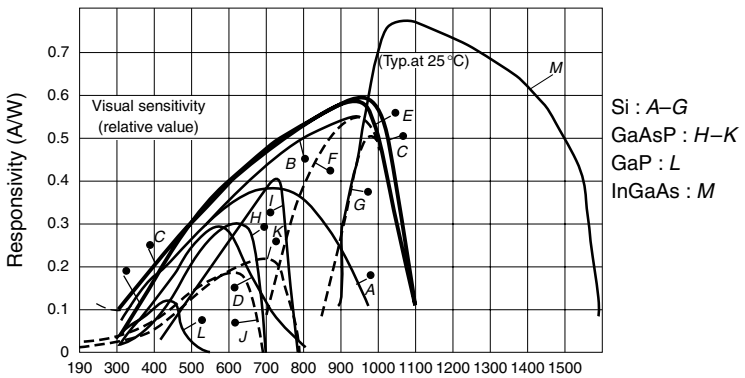

(b)

Figure 12.6 Spectral response of the PIN photodiode and APD. (a) Generic spectral response of the PIN photodiode and APD. (b) Spectral response of photodiodes. (After Hamamatsu Photonics catalog).

than linearly at shorter wavelengths due to scattering and deviation from the center frequency of the designed antireflection coating. Figure 12.6b shows the sensitivity of various semiconductor detectors. The wavelength dependence of η varies with the semiconductor material. The wavelength regions for optimum sensitivity are:

Ge	0.8–1.6 μm
Si	0.5–0.9 μm
InGaAs	1.0–1.6 μm

As with the photomultiplier, the responsivity is used to characterize a photodiode.

The output current with unit incident light power is the responsivity R, and R is expressed as

$$R = \eta \frac{e}{hv} M \tag{12.9}$$

or

$$i = RP \tag{12.10}$$

The responsivity of most PIN diodes is 0.5 A/W and a good rule of thumb is that every 1 watt of incident light power generates $\frac{1}{2}$ ampere of output current.

The reasons why the PIN photodiode and APD are exclusively used for fiber-optic communications are that both have (1) high photoelectric conversion efficiency, (2) fast response time, (3) high reliability, (4) compactness as well as ruggedness, (5) longevity, (6) simple electronics, (7) moderate cost, and (8) high linearity of output current over a wide range of input light power.

The rest of the chapter concentrates on how to incorporate these photodiodes in fiber-optic communication systems that are broadly categorized as direct detection systems and coherent detection systems.

12.5 DIRECT DETECTION SYSTEMS

Figure 12.7 shows a very basic circuit employing a PIN photodiode for direct detection in a fiber-optic communication system. The photodiode is back-biased. The p layer is negative, and the n layer is positive. The bias voltage is in the range of 7–15 volts. The capacitor C prevents the signal from going through the power supply. This particular circuit is connected directly to a transistor amplifier, but a more sophisticated coupling circuit is required if impedance matching, frequency response, and signal to noise ratio are all to be considered. The details for these more sophisticated circuits are presented in Chapter 16.

Let the instantaneous E field of the light incident to the photodiode be

$$E_s = S(t)\cos(\omega_c t + \theta) \tag{12.11}$$

where $S(t)$ is the modulated amplitude, ω_c is the carrier frequency of the light, and θ is either the modulated or unmodulated phase angle of the carrier. In order to calculate the detected signal current i_s using Eq. (12.8), the input power P_s has to be calculated.

The peak energy per unit time crossing a unit area is, by the Poynting vector theorem,

$$\mathbf{S} = \mathbf{E} \times \mathbf{H} \tag{12.12}$$

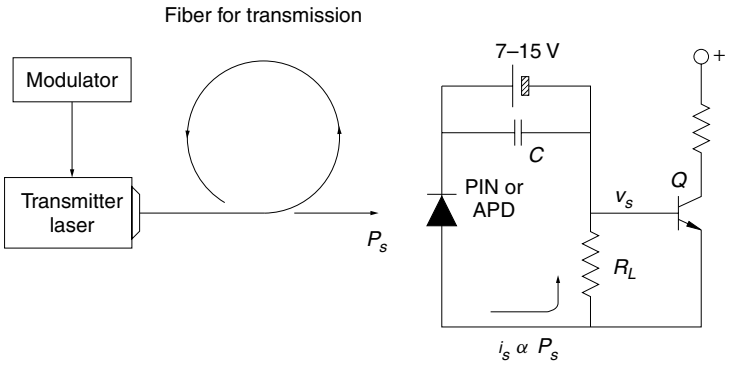

Figure 12.7 Direct detection system.

The magnitude of **E** and **H** have the relationship

$$E = \eta_0 H$$

where η_0 is the intrinsic impedance. The average energy per unit time crossing area s is

$$\begin{aligned} P_s &= \frac{s}{\eta_0}\langle E_s^2 \rangle \\ &= \frac{s}{\eta_0} S^2(t)\langle \cos^2 \omega_c t \rangle \\ &= \frac{s}{2\eta_0} S^2(t) \end{aligned} \tag{12.13}$$

where $\langle \quad \rangle$ is the time average over a length of time containing a large number of light carrier periods but not so large a number in modulation periods. The detected signal current from the avalanche photodiode can be expressed in various ways:

$$\begin{aligned} i_s &= \frac{\eta e}{h\nu} M P_s \\ &= \frac{\eta e}{h\nu} M \frac{s}{2\eta_0} S^2(t) \\ &= R \frac{s}{2\eta_0} S^2(t) \\ &= K S^2(t) \end{aligned} \tag{12.14}$$

where

$$K = \frac{e\eta}{h\nu} M \frac{s}{2\eta_0}$$

Expressions in terms of the light amplitude $S(t)$ rather than the power P_s are more convenient for explaining mixer operations. The amplitude constant K accounts for both responsivity and sensor area and directly relates the amplitude square to the output current from the diode.

Note that i_s is proportional to the light intensity and does not contain information about either the frequency ω_c of the light carrier or the phase ϕ. Thus, direct detection cannot be used for detecting frequency modulated or phase modulated signals.

The mean square value of the direct detection signal is

$$\langle i_s^2 \rangle = \left(\frac{\eta e}{h\nu} M\right)^2 P_s^2 \tag{12.15}$$

Next, coherent detection systems that can be used not only with intensity modulated light but also with phase and frequency modulated light are presented.

12.6 COHERENT DETECTION SYSTEMS

Four more schemes besides the direct detection scheme will be explained here. These four are coherent detection schemes [6,7] and are so named because they require a local oscillator laser whose output light is either coherent or quasicoherent with the signal light. Making a comparison with a radio receiver set, direct detection is analogous to a crystal radio. The crystal radio is simple, but the sensitivity and station selectivity are poor. Direct detection is primarily used for an on–off type of modulation. Coherent optical detection is analogous to a superheterodyne radio. The superheterodyne radio is much more sophisticated, but its sensitivity and selectivity are far better than the crystal radio.

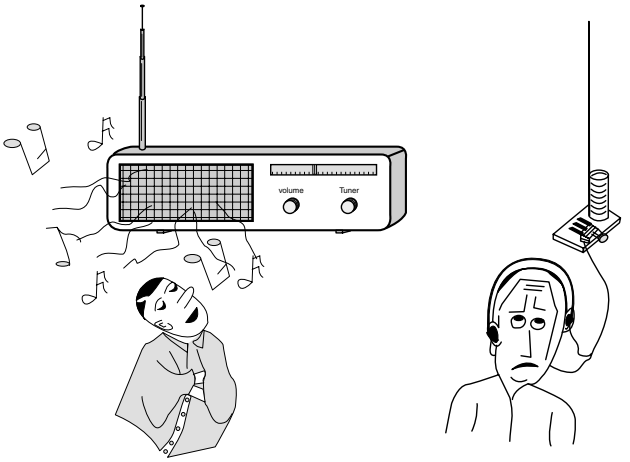

12.6.1 Heterodyne Detection

Optical heterodyne detection [8,9] uses the beat signal between the signal light and the local oscillator (LO) light.

Figure 12.8 shows a heterodyne detection circuit. The signal light from the transmitter laser passes through the fiber-optic cable transmission line and prior to being combined with the local oscillator laser light, the signal light passes through a polarization controller. The polarization controller adjusts the state of polarization of the signal light so that it is linearly polarized in the desired direction with respect to the local oscillator laser light (parallel in the case of a single mixer). The frequency difference between the local oscillator laser and the signal light has to be maintained at a constant

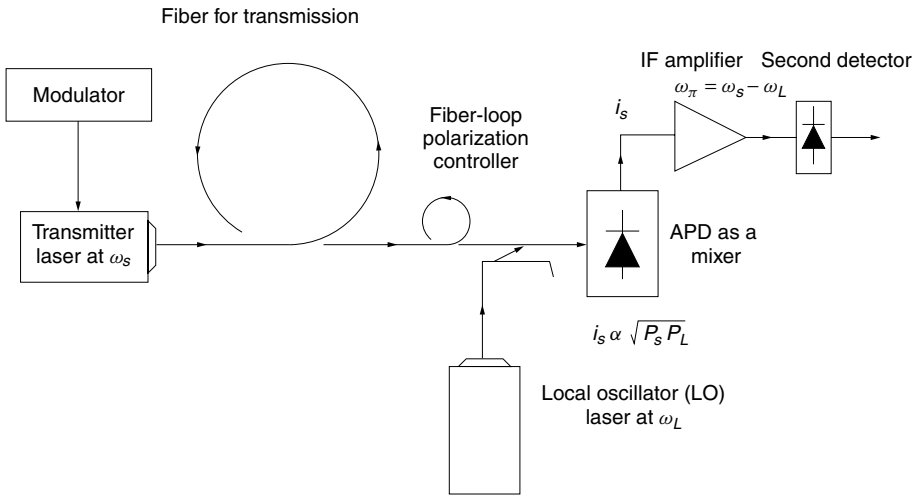

Figure 12.8 Heterodyne detection.

value. The output from the mixer is amplified by an IF amplifier and then detected a second time to recover the desired information from the IF signal.

The field at the mixer surface is the sum of the received signal field and the local oscillator laser field. Let the incident light be the same as the case of direct detection given by Eq. (12.11) and let the local oscillator laser light be

$$E_L = E_{\text{LO}} \cos(\omega_L t + \theta_L) \tag{12.16}$$

Both the signal and local laser light illuminate the APD diode used as a mixer diode. The resultant incident light power is obtained from the top equation of Eq. (12.13) replacing E_s by $E_L + E_s$.

$$P = \frac{s}{\eta_0} \langle [S(t) \cos(\omega_c t L) + E_{\text{LO}} \cos(\omega_L t + \theta_L)]^2 \rangle \tag{12.17}$$

Using Eq. (12.8) and the identity $\cos x \cos y = \frac{1}{2}[\cos(x - y) + \cos(x + y)]$, the output current from the mixer is

$$i_{\text{IF}} = \frac{\eta e}{h\nu} M \{P_s + P_L + 2\sqrt{P_s P_L} \cos[\omega_{\text{IF}} t + (\theta_c - \theta_L)]\} \tag{12.18}$$

where

$$\omega_{\text{IF}} = \omega_c - \omega_L, \qquad P_s = \frac{s}{2\eta_0} S^2(t), \qquad P_L = \frac{s}{2\eta_0} E_{\text{LO}}^2 \tag{12.19}$$

and where ω_L and ω_{IF} are the local oscillator and IF frequencies, respectively. The terms with $(\omega_c + \omega_L)$ have been ignored. The phases of the signal and local oscillator light are θ_c and θ_L, respectively. Only the third term of Eq. (12.18) contains the signal at the intermediate frequency ω_{IF}. The mean square value of the IF signal is, from Eq. (12.18),

$$\langle i_{\text{IF}}^2 \rangle = 2 \left(\frac{\eta e}{h\nu} M \right)^2 P_s P_L \tag{12.20}$$

The mean square value of the IF signal is the product of the signal and local oscillator powers, while that of the direct detection system as given by Eq. (12.15) is the square of the signal power, which for weak signals is the square of an already small quantity. Thus, the output from the heterodyne detection for the small signal case is significantly higher than that of direct detection. The selectivity of the heterodyne system is also higher than that of direct detection because the bandwidth of the heterodyne is determined by the bandwidth of the IF amplifier, which is a lower frequency and can be tailored to the required bandwidth of the signal more easily, typically in the gigahertz range. This not only improves the selectivity but enhances the rejection of the noise power. Direct detection, on the other hand, has to rely on an optical bandpass filter (whose bandwidth is normally much wider than gigahertz) for wavelength selectivity and noise power rejection.

12.6.2 Homodyne Detection

When the frequency of the local oscillator of the heterodyne detection system [10,11] is made equal to the frequency of the signal light, the system becomes homodyne. The homodyne system not only relaxes the frequency bandwidth requirement of the IF amplifier but also improves the sensitivity by 3 dB over heterodyne detection. The phase stability requirement of the local oscillator, however, is severe and an elaborate phase stabilization circuit is required for the local oscillator laser.

With

$$\omega_c = \omega_L \quad \text{or} \quad \omega_{\text{IF}} = 0$$

Eq. (12.18) becomes

$$i_m = \frac{\eta e}{h\nu} M[P_s + P_L + 2\sqrt{P_s P_L}\cos(\theta_c - \theta_L)] \tag{12.21}$$

When P_L is large in comparison to P_s, the third term is the signal component. The phase-lock loop assures $\theta_c = \theta_L$ for the steady signal. The mean square value of the desired signal is

$$\langle i_m^2 \rangle = 4\left(\frac{\eta e}{h\nu} M\right)^2 P_s P_L \tag{12.22}$$

Compare this result with the heterodyne result in Eq. (12.20). There is a factor of 2 difference. This difference comes from averaging $\langle \cos^2[\omega_{\text{IF}} t + (\theta_c - \theta_L)] \rangle$ in Eq. (12.18), which is $\frac{1}{2}$ and averaging $\langle \cos^2(\theta_c - \theta_L) \rangle$ in Eq. (12.21), which is unity for $\theta_c = \theta_L$. Thus, the signal to noise ratio and hence the sensitivity of the homodyne system is better than the heterodyne system by 3 dB.

A disadvantage of homodyne detection is the stringent requirement on the phase stability of both the transmitting and local oscillator lasers. In Eq. (12.21), if $(\theta_c - \theta_L)$ fluctuates between 0° and 90°, the output fluctuates between its maximum value and zero, and communication becomes impossible. A phase-lock loop (PLL) can extract the carrier frequency component from the amplitude modulated carrier. The extracted carrier is used to lock the oscillation of the local oscillator signal.

Figure 12.9 shows a block diagram of the Costas PLL [12]. Inside the 90° optical hybrid, the local oscillator signal is divided into two components, one of which is phase

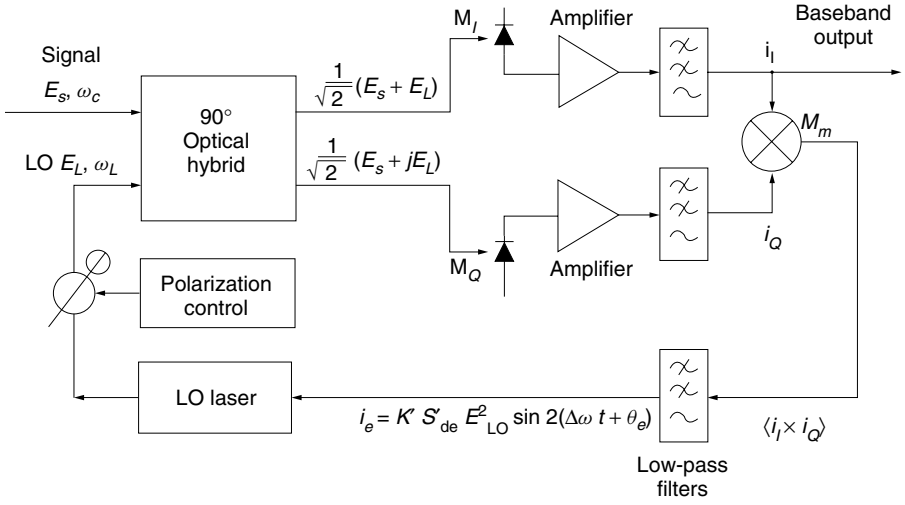

Figure 12.9 Homodyne detection with a phase-lock loop.

shifted by 90°. The component with the same phase as the original local oscillator signal and that with a 90° phase shift are expressed as

$$\begin{aligned} E_{L_I} &= \frac{1}{\sqrt{2}} E_{\mathrm{LO}} \cos(\omega_L t + \theta_L) \\ E_{L_Q} &= \frac{1}{\sqrt{2}} E_{\mathrm{LO}} \sin(\omega_L t + \theta_L) \end{aligned} \tag{12.23}$$

The local oscillator power P_L is assumed to be equally divided into the two components. The subscripts I and Q stand for in-phase and quadrature, respectively. The two components of the local oscillator are separately mixed with the received signal at mixers M_I and M_Q. When E_{L_I} is fed into M_I with the received signal, the output from M_I is similar to Eq. (12.18). The IF component of the output current is i_I. Similarly, the output from M_Q is i_Q. The $\Delta\omega$ components of the outputs from M_I and M_Q are called the in-phase and quadrature components of the IF signal. They are given by

$$\begin{aligned} i_I &= \sqrt{2} K S(t) E_{\mathrm{LO}} \cos(\Delta\omega\, t + \theta_e) \\ i_Q &= \sqrt{2} K S(t) E_{\mathrm{LO}} \sin(\Delta\omega\, t + \theta_e) \end{aligned} \tag{12.24}$$

where

$$\Delta\omega = \omega_c - \omega_L, \qquad \theta_e = \theta_c - \theta_L$$

and K is given by Eq. (12.14). Now, both i_I and i_Q are fed into another mixer M_m. The relevant component of the output from the mixer is

$$i_e = \tfrac{1}{2} K' 2[S(t) E_{\mathrm{LO}}]^2 \sin 2(\Delta\omega\, t + \theta_e) \tag{12.25}$$

where K' is a constant associated with the electronic mixer. $[S(t)]^2$ can be rewritten as

$$[S(t)]^2 = S_{\text{dc}} + S_{\text{ac}}\ (t) \tag{12.26}$$

where S_{dc} is the average component and $S_{\text{ac}}\ (t)$ is the ac component of $[S(t)]^2$. The frequency spectrum of $S_{\text{ac}}\ (t)$ is associated with the modulation by the signal and is normally much higher (tens of gigahertz) than $\Delta\omega$, provided ω_L is close to ω_c. With a low-pass filter, $S_{\text{ac}}\ (t)$ can be removed. The output of the low-pass filter becomes

$$i_e = K_1' E_{\text{LO}}^2 S_{\text{dc}} \sin 2(\Delta\omega\ t + \theta_e) \tag{12.27}$$

The output i_e from the mixer is used as an error signal to control the frequency and phase of the local oscillator laser diode. To explain the operation, assume first that the frequency is already matched but the phase is not: $\Delta\omega = \omega_c - \omega_L = 0$ and $\theta_e = \theta_c - \theta_L \neq 0$. Figure 12.10 shows a plot of the error signal i_e as a function of the phase mismatch θ_e.

Consider only the region of $-\pi/4 < \theta_e < \pi/4$. Let us say the operating point is at P in Fig. 12.10. A positive value of the error signal i_e means $\theta_e > 0$ or $\theta_c > \theta_L$. A positive error signal i_e raises the local oscillator frequency higher so that θ_L is increased and reaches the value of θ_c, thereby bringing the operating point P to the origin.

Next, suppose that ω_c makes an abrupt increase $\Delta\omega$ at $t = 0$. In this case, $\theta_e = \Delta\omega\, t$ starts to increase, and hence i_e starts to increase, raising the local oscillator frequency ω_L in order to catch up with the increase in ω_c and bring the operating point back to the origin. It is, however, crucial that the turnaround time of this feedback process be fast enough to react before θ_e goes beyond the range of $\pm\pi/4$ radians.

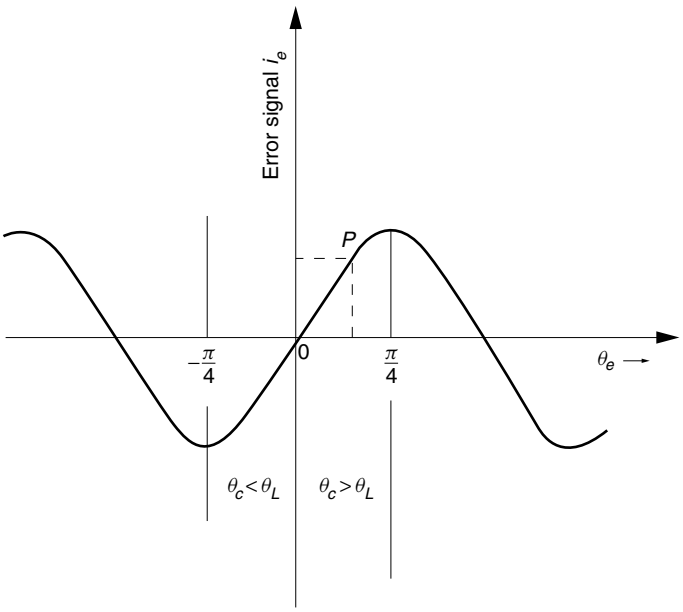

Figure 12.10 Error signal $\langle i_I i_Q \rangle_{\text{error}}$ as a function of phase error $\theta_e = \theta_c - \theta_L$.

In the case of ASK ("on–off") modulation, either the in-phase or the quadrature component alone of Eq. (12.24) could have been used directly as an error signal to the feedback loop. For phase modulation, where $S(t)$ takes on positive and negative values (or 0° and 180° phases), the sign of the error signal changes as $S(t)$ changes sign, and both in-phase and quadrature components had to be used as the error signal.

In this way, the phase as well as the frequency of the local oscillator is locked to the received carrier frequency. In other words, the local oscillator is completely coherent with the received signal, and in traditional communication theory, only homodyne is called coherent detection. In the field of optics, both heterodyne and homodyne are generally called coherent detection.

12.6.3 Intradyne System

The intradyne system [10] is a hybrid of the heterodyne and homodyne systems. It enjoys the merits of both systems. The stringent requirements on the frequency bandwidth and phase stability are relaxed. The intradyne system normally incorporates the phase diversity technique in which the signal is first divided into more than one channel before detection. Signal processing circuits, such as squaring and differentiating circuits, are installed in each channel. After being processed, the signals from the divided channels are added to render a final signal that is free from phase jitter.

In the homodyne system shown in Fig. 12.9, if the local oscillator frequency is not completely matched, both the in-phase, i_I, and quadrature, i_Q, components become modulated at a frequency $(\omega_c - \omega_L)$ as shown in Figs. 12.11c and 12.11d. Such outputs can almost be used as the final signal, but modulation of the amplitude at frequency $\Delta\omega = (\omega_c - \omega_L)$ creates a problem.

The intradyne system shown in Fig. 12.12 uses both in-phase and quadrature components to remove the modulation of the amplitude. The sum of the squares of the in-phase component and the quadrature component, Eq. (12.24), gives the output

$$i^2 = 2[KE_{\mathrm{LO}}S(t)]^2 \tag{12.28}$$

i^2 is free from $(\omega_L - \omega_c)$ and ϕ. The quadrature current i_Q is fed to the frequency discriminator, which keeps $(\omega_L - \omega_c)$ within a given range. Such an intradyne detector is sometimes called a phase diversity receiver because two phase components are used. It should be noted that the output being $2K^2E_{\mathrm{LO}}^2S^2(t)$, this detection system is not suitable for either phase or frequency modulated signals.

It is also possible to split the signal into N components with equal phase spacing between components. But, the larger N is, the higher the local oscillator power is needed. The loss in the circuit is also increased. An advantage of a larger N, however, is that uniformity among the channels is less critical.

As already mentioned, the frequency of the input light is converted into either an IF or baseband signal by mixing the incoming signal with the local oscillator light. The quality of the mixer significantly influences the sensitivity of the heterodyne system because the mixer is the first element that the signal at its lowest power level sees. Because of this importance, the function of the mixer will be explained in detail here.

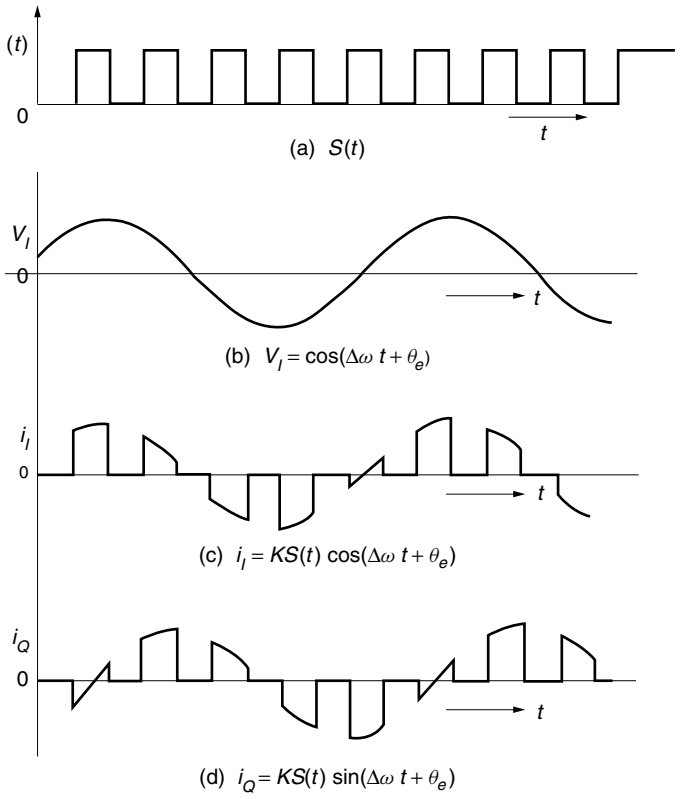

Figure 12.11 Intradyne signal.

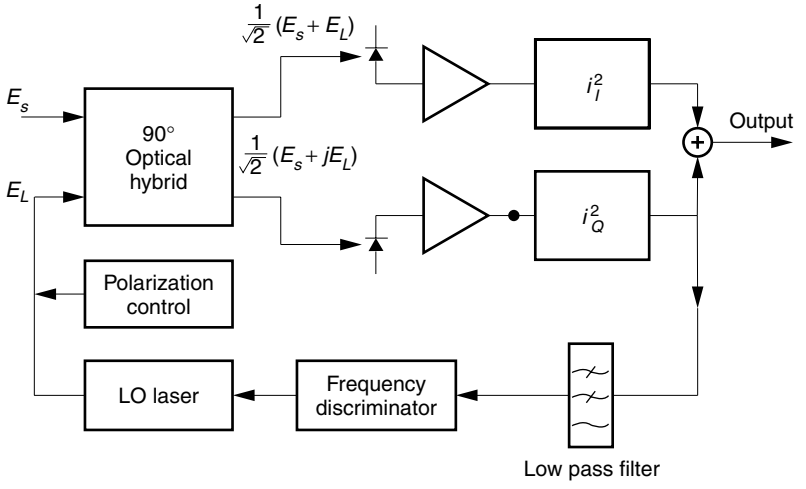

Figure 12.12 Intradyne detection.

12.7 BALANCED MIXER

There are two types of mixers: the single crystal mixer as shown in Fig. 12.13a, and the double balanced mixer [13] as shown in Fig. 12.13b.

The most commonly used input elements to the mixer are optical fiber couplers or prism couplers. The substrate optical coupler shown in (1) of Fig. 12.13b will be treated. Assume that inside the substrate optical coupler, the field that crosses the guide from the upper to lower or from the lower to upper guide experiences a 90° phase shift compared to the field that goes straight through. The input fields E_1 to mixer M_1 and E_2 to mixer M_2 will be calculated first. The 90° phase shift will be accounted for by changing the cosine function into a sine function. The input fields to the mixers are expressed as

$$E_1 = \frac{1}{\sqrt{2}}[S(t)\cos\omega_c t + E_{\mathrm{LO}}\sin\omega_L t] \tag{12.29}$$

$$E_2 = \frac{1}{\sqrt{2}}[S(t)\sin\omega_c t + E_{\mathrm{LO}}\cos\omega_L t] \tag{12.30}$$

where $S(t)$ and E_{LO} are the signal and local oscillator fields, respectively. The factor $1/\sqrt{2}$ is necessary because the light power is split 50–50.

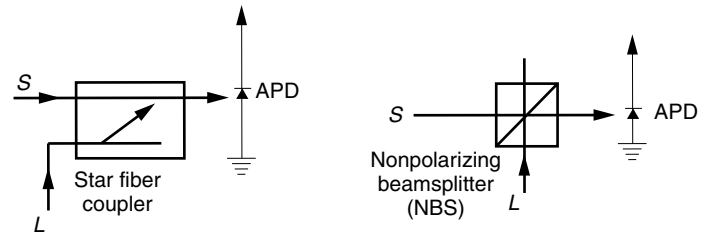

(1) Star fiber coupling (2) Nonpolarizing beamsplitter coupling

(a)

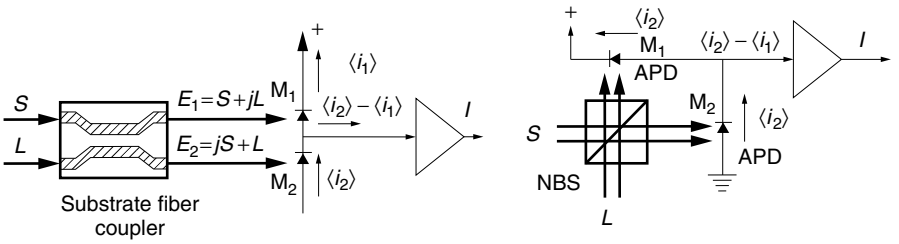

(1) Fiber coupling (2) Prism coupling

(b)

Figure 12.13 Comparison between (a) the single crystal mixer and (b) the double balanced mixer.

The output currents i_1 and i_2 from mixer M_1 and mixer M_2 are

$$\langle i_1 \rangle = K_1 \left[\tfrac{1}{2} S^2(t) - S(t) E_{\mathrm{LO}} \sin(\omega_c - \omega_L)t + \tfrac{1}{2} E_{\mathrm{LO}}^2 \right] \tag{12.31}$$

$$\langle i_2 \rangle = K_2 \left[\tfrac{1}{2} S^2(t) + S(t) E_{\mathrm{LO}} \sin(\omega_c - \omega_L)t + \tfrac{1}{2} E_{\mathrm{LO}}^2 \right] \tag{12.32}$$

Equation (12.31) or (12.32) alone is the expression for the output current from the single crystal detection. If the intensity of the local oscillator laser fluctuates, the mixer output fluctuates accordingly, and the fluctuations in E_{LO}^2 become a source of noise.

In a double balanced mixer, however, i_1 is subtracted from i_2. This means both first and third terms in Eqs. (12.31) and (12.32) cancel each other,* provided the quantum efficiencies of the two mixers are well balanced and

$$\eta_1 = \eta_2 = \eta \quad \text{and hence} \quad K_1 = K_2 = K \tag{12.33}$$

Assuming Eq. (12.33) is valid, the output from the double balanced mixer is

$$i = 2KS(t)E_{\mathrm{LO}} \sin \omega_{\mathrm{IF}} t \tag{12.34}$$

The signal current in Eq. (12.34) is indeed double that of the single crystal mixer given by Eq. (12.31) or (12.32).

Fluctuations in E_{LO} will cause i to fluctuate, but the amount is different for the two cases. Equation (12.31) for the single mixer contains a term proportional to E_{LO}^2, whereas Eq. (12.34) for the double mixer is proportional to $S(t)E_{\mathrm{LO}}$. Normally, $S(t)$ is significantly weaker than E_{LO}, so that the effect of local oscillator fluctuations is significantly improved over the case of the single crystal mixer.

Even though the double balanced mixer is more complicated in structure than the single crystal detector, it has such advantages as:

1. The output signal current is twice as much as that from the single crystal mixer.
2. The mixer output is practically free from the noise generated by the intensity fluctuations of the local oscillator laser.
3. Even when the output of the mixer is dc coupled to the preamplifier, saturation of the preamplifier can be avoided because of the absence of the dc current.

Next, a method of detection that resembles none of the above will be explained.

12.8 DETECTION BY STIMULATED EFFECTS

Another unique method of detection is the use of the stimulated effect in the optical fiber. It can be considered as a kind of homodyne detection whose local oscillator light is generated by stimulated Brillouin scattering (SBS) inside the optical fiber during transmission. Such a scheme does not require phase stabilization of the local oscillator because the signal induced by the stimulated Brillouin scattering is automatically in phase with the carrier of the signal. It also provides an additional gain of 15–25 dB during transmission. A drawback, however, is that stimulated Brillouin scattering cannot be effectively suppressed during the "off" period of the ASK modulation.

* The $S(t)E_{\mathrm{LO}} \sin(\omega_C + \omega_L)t$ terms were not included in Eqs. (12.31) and (12.32) because they are outside the spectral range of interest. Even if they had been included, these terms would cancel each other when i_1 is subtracted from i_2.

12.8.1 Stimulated Effects

Detection associated with the nonlinear effect of the glass will be explained [14–18]. When a light beam with a diameter of a few millimeters is focused into the core of an optical fiber with a diameter of a few micrometers, the light intensity is increased by 10^6 times. When one compares the length of an optical fiber with the lengths of other optical components, the fiber is typically 10^4 times longer. The power density-interaction length is used as a barometer of the enhancement of the nonlinear effect. An optical fiber is 10^{10} times more susceptible to nonlinear effects than a bulk optical component.

Close observation reveals that even when monochromatic incident light is used, the spectrum of the light reflected back from inside the fiber is no longer monochromatic. This phenomenon is quite different from the electrooptic effect that relates to the change in the index of refraction but does not involve a change in frequency spectrum.

As shown in Fig. 12.14, on both sides of the spectrum of the incident light, two new lines become observable as the intensity of the incident light is raised. Spectra appearing on the lower frequency side are called lines of Stokes radiation, and those appearing on the higher frequency side are called lines of anti-Stokes radiation. The ratio of the intensity I_S of Stokes radiation to the intensity I_a of anti-Stokes radiation obeys the Boltzmann distribution and

$$I_a/I_S = e^{-2h\Delta f/kT} \tag{12.35}$$

where Δf is the frequency shift of the Stokes wave. Thus, the intensities of the Stokes waves are larger than those of the anti-Stokes waves.

Both Stokes and anti-Stokes waves consist of two sets of spectral lines. One is due to Brillouin scattering and the other is due to Raman scattering. The mechanism

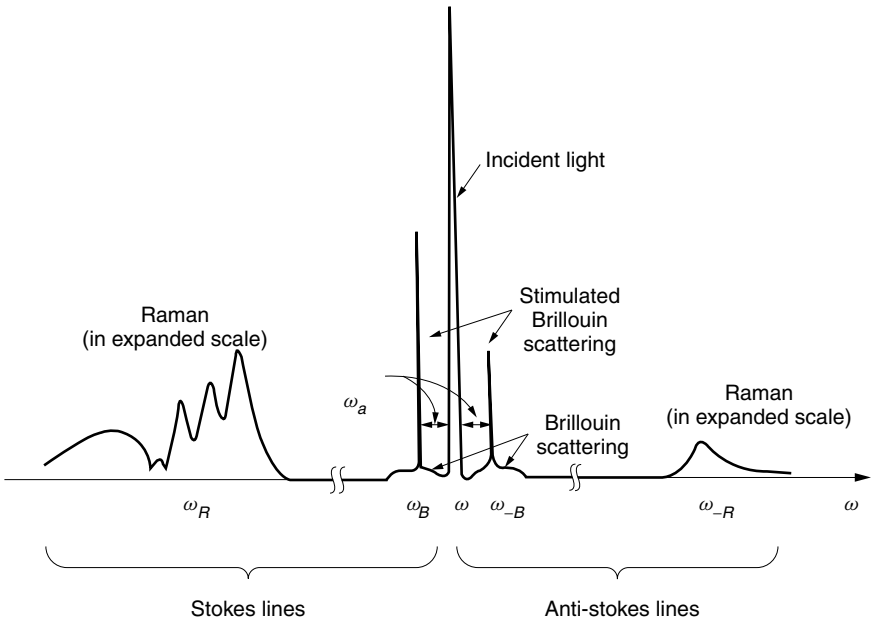

Figure 12.14 Typical Stokes and anti-Stokes lines.

of the frequency shift for Brillouin and Raman scatterings are different. While Raman scattering is associated with vibrations of dipole moments formed by two ions in a unit cell of the crystal lattice, Brillouin scattering is the reflection of light from acoustic waves (phonons) generated by the electrostrictive effect. The characteristics of the Brillouin scattering are different from that of the Raman scattering.

12.8.2 Homodyne Detection by Stimulated Brillouin Scattering

Figure 12.15 shows a block diagram of a homodyne receiver that uses the wave generated by stimulated Brillouin scattering (SBS). The pump laser light with a power of several milliwatts at frequency ω_L is injected from the receiver end into the optical fiber in the reverse direction from that of the signal flow. The signal light is much weaker in intensity compared to the pump. A beat wave is generated between the pump laser light at ω_L and the signal wave whose carrier frequency ω_s is set to be identical with the frequency ω_B of the Brillouin scattering. Two waves traveling in opposite directions but with slightly different frequencies generate a "moving" standing wave in the fiber in the direction of propagation of the higher carrier frequency light. This "moving" standing wave generates an acoustic wave due to the electrostrictive effect. The acoustic wave spatially modulates the index of refraction of the core. Consequently, a moving optical grating is formed in the core. If the Bragg condition is satisfied, the moving optical grating efficiently scatters the pump beam into the same direction as the signal, creating a second beam heading toward the receiver. The frequency of the second wave is shifted lower with respect to that of the pump beam due to the Doppler effect of the moving scatterer (SBS). This second beam has the same frequency as the signal light. The net result is an increase in the signal power.

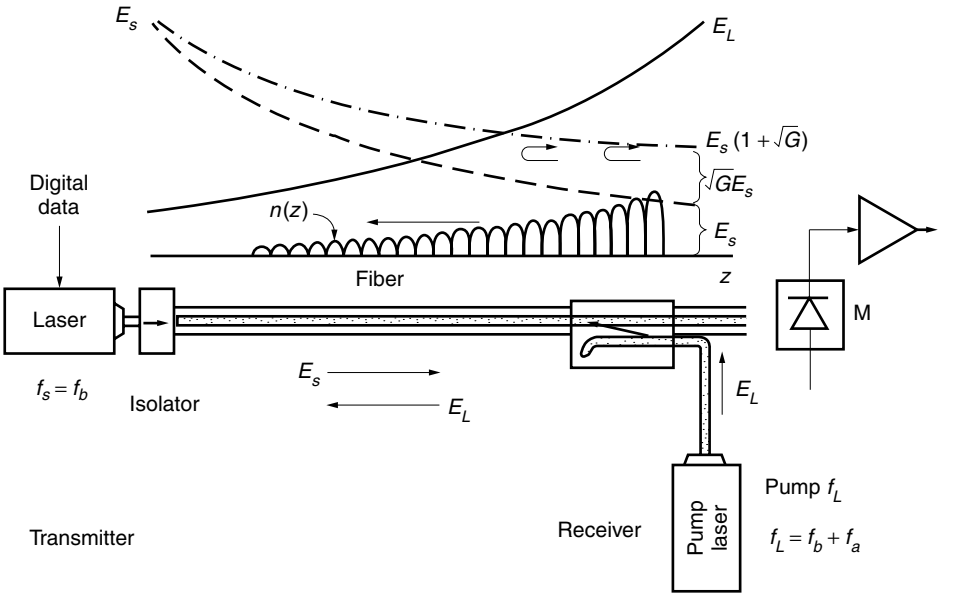

Figure 12.15 Homodyne receiver based on stimulated Brillouin scattering.

This amplification is immune to the phase jitter of the signal. If the phase of the signal is delayed by $\Delta\phi$ radians, the peak positions of the grating shift by $d = \frac{1}{2}\Delta\phi/\beta$ toward the source. The local oscillator signal reflected from the grating has to travel an extra distance $2d$, causing a phase delay of $2d\beta = \Delta\phi$. Thus, the reflected local oscillator signal is delayed by the same amount. Thus, the secondary beam has both the same frequency and the same phase. Two special features of this amplification are the automatic synchronization of the phase of the pump beam with that of the signal beam and the narrowness of the frequency bandwidth, typically 20 MHz. Thus, this phenomenon can play the role of the synchronous homodyne receiver.

This scheme not only detects the signal but also has a power gain of G that is proportional to the pump power and is typically 15–25 dB. The drawback is the difficulty in applying ASK modulation (on–off modulation) because the stimulated Brillouin scattering tends to continue even during the light off period of the on–off modulation.

Let us find the frequency relationships. The frequency f_B of Brillouin scattering that will beat with a frequency f_L of the pump light and generate the acoustic frequency f_a is

$$f_L - f_B = f_a \tag{12.36}$$

The grating has to satisfy the Bragg condition if the reflected wave is enhanced by Brillouin scattering. If the acoustic wave propagates at velocity V_a in the crystal, the

When two atoms in a unit crystal cell consist of positive and negative ions, these two atoms form an electric dipole. Such a dipole oscillates when an oscillating external field **E** is applied. The oscillating dipole in turn reradiates an electromagnetic wave. Such a dipole has a resonant frequency ω_v of oscillation that is determined, among other physical parameters, by the atomic weight. When the frequency ω_v of the external field coincides with this resonant frequency, the intensity of the reradiation is greatly enhanced. If, as a start, a small-intensity signal at ω_R in the thermal noise spectrum is mixed with the frequency ω_L of the external field in the nonlinear medium, beat waves are generated at the sum frequency $\omega_L + \omega_R$ and the difference frequency $\omega_L - \omega_R$. Only the frequency ω_R in the thermal noise spectrum that satisfies

$$\omega_L - \omega_R = \omega_v$$

can effectively excite the dipole. The reradiated field at ω_v from the dipole again mixes with the incident wave at ω_L and contributes to the signal field at frequency ω_R. The cyclic reaction repeats and builds up the signal at ω_R. To summarize, the incident energy at ω_L is transferred into the Raman spectrum at ω_R using the ionic dipole and the nonlinear properties of the medium.

The amplification based on the stimulated Raman scattering (SRS) goes through the same procedure but the difference is that the spectrum ω_R is injected rather than that originating from the thermal noise spectrum. The intensity of the output at ω_R is larger than that of the input power due to the enhancement of the Raman scattering. Such an enhancement can be used for a Raman amplifier or a Raman oscillator [19,20].

The intensity of Stokes radiation due to Raman scattering in a SiO_2 fiber is about two orders of magnitude smaller than that of Brillouin scattering. The frequency shift of the spectrum due to Brillouin scattering is 11.4 GHz while that of Raman scattering is about a few hundred terahertz. The linewidth of Raman scattering is of the order of terahertz, while that of stimulated Brillouin scattering is of the order of tens of megahertz.

wavelength λ_a of the acoustic wave is $\lambda_a = V_a/f_a$. For the pump wave to satisfy the Bragg condition, λ_a has to be one-half of the wavelength of the pump light:

$$\frac{1}{2}\frac{c}{n}\cdot\frac{1}{f_L} = \frac{V_a}{f_a} \tag{12.37}$$

Now, the value of f_B that satisfies both Eqs. (12.36) and (12.37) is

$$f_B = f_L\left(1 - \frac{2n}{c}V_a\right) \tag{12.38}$$

Thus, the frequency of the Brillouin scattering is shifted by $(2n/c)V_a f_L$, which is much smaller than f_L because V_a/c is quite small. For the case of a fused silica fiber, $V_a = 5960$ ms^{-1}, $\lambda_L = 1.5$ μm, and $n = 1.44$. The frequency difference between the signal and the local oscillator is 11.4 GHz.

12.9 JITTER IN COHERENT COMMUNICATION SYSTEMS

The two kinds of jitter (unpredictable change) that impact coherent communication systems are polarization jitter and phase jitter. The presence of these jitters will cause the output signal to wax and wane. If the jitter is severe enough, there will be times when the signal fades completely, thus interrupting communication. Countermeasures have to be incorporated.

12.9.1 Polarization Jitter Controls

When linearly polarized light is sent through a fiber that does not preserve the state of polarization of the input light, the received signal is generally elliptically polarized. For optimum mixing, the state of polarization of both the received signal and the local oscillator signal should match. A means of adjusting the state of polarization of one or the other is required.

Polarization-maintaining fibers could be used in place of polarization controllers; however, this is not always an option when using existing cables that have been installed with non-polarization-maintaining fiber.

The fiber-loop polarization controller described in Chapter 6 can be used to convert the polarization of the received light into a state that is linearly polarized parallel to the local oscillator light. However, the fiber-loop polarizer [21,22] cannot cope with a fluctuating state of polarization. In ordinary optical fibers, the polarization is apt to change over time because of changes in stress caused by temperature changes or by mechanical vibration of the transmission fiber [23]. An automatic polarization control is necessary to dynamically correct for changes in polarization.

Example 12.1 Both the signal and the local oscillator signals are linearly polarized, but they are not parallel to each other on the input surface of the mixer. What is the IF output current when they are angled spatially at ϕ as shown in Fig. 12.16?

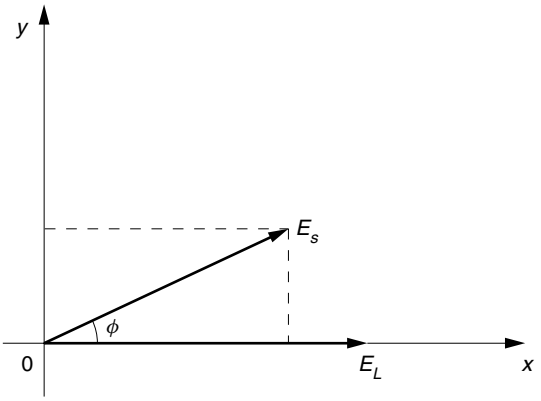

Figure 12.16 IF output current when E_S and E_L have a separation angle of ϕ.

Solution Let us say the input signal and local oscillator signal are

$$\begin{aligned} E_s &= S(t)\cos(\omega_c t + \theta) \\ E_L &= E_{\text{LO}}\cos\omega_L t \end{aligned} \tag{12.39}$$

The component of the signal parallel to the local oscillator is $E_s \cos\phi$ and that of the perpendicular component is $E_s \sin\phi$.

The output from the mixer is proportional to the power or square of the resultant **E** field, which is the sum of the squares of resultant fields parallel and perpendicular to the local oscillator field.

$$\begin{aligned} i &= 2K\langle[E_{\text{LO}}\cos\omega_L t + S(t)\cos\phi\cos(\omega_c t + \theta)]^2 \\ &\quad + [S(t)\sin\phi\cos(\omega_c t + \theta)]^2\rangle \\ &= 2K\left[\frac{1}{2}E_{\text{LO}}^2 + \frac{1}{2}S^2(t) + E_{\text{LO}}S(t)\cos\phi\cos(\omega_{\text{IF}}t + \theta)\right] \end{aligned} \tag{12.40}$$

Thus, the IF current component is the third term in Eq. (12.40).

$$i_{\text{IF}} = 2KE_{\text{LO}}S(t)\cos\phi\cos(\omega_{\text{IF}}t + \theta) \tag{12.41}$$

In conclusion, only the field component that is parallel to the local oscillator field contributes to the IF current. □

There are two approaches for automatically correcting the state of polarization. These are the computer-controlled method and the polarization diversity method. As evident from the name, the computer-controlled approach corrects the polarization of the received signal through computer control. The polarization diversity method uses an analog circuit that can process the signal independent of the state of polarization.

12.9.1.1 Computer-Controlled Method of Jitter Control

A designated computer either searches for the maximum output by interrogating the reaction to a small perturbation of the control signal, or actually monitors the state of

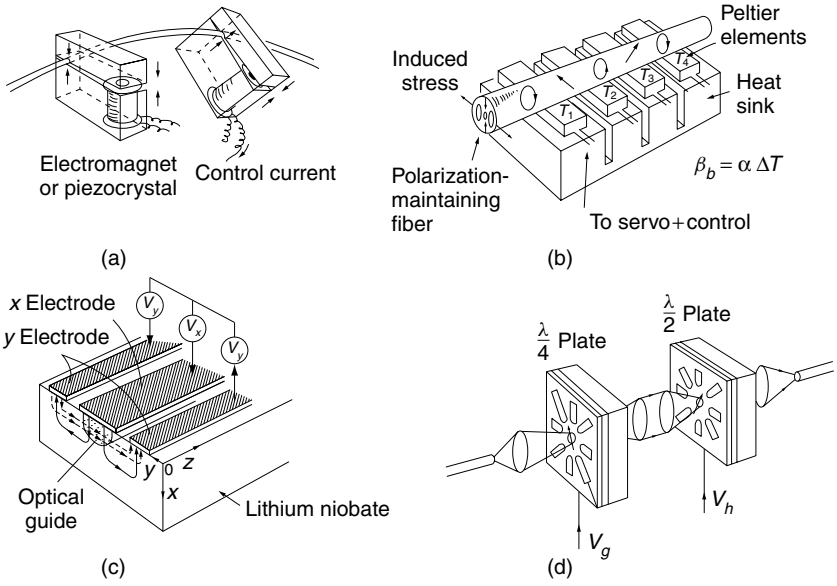

Figure 12.17 Various types of automatic polarization controller elements. (a) Based on squeezing the fiber. (After A. S. Siddiqui and Y. Aihua [25].) (b) Based on heat. (After N. G. Walker and G. R. Walker [26].) (c) Based on the electrooptic effect. (After N. G. Walker and G. R. Walker [26].) (d) Electrically rotatable liquid crystal waveplates. (After T. Chiba, Y. Ohtera, and S. Kawakami [29].)

polarization at an intermediate stage and issues commands to the appropriate elements. In either way, elements are needed whose birefringence can be computer controlled [24]. Figure 12.17 shows examples of such elements.

The fiber squeezer polarization controller [25] makes use of the stress-induced birefringence created by squeezing the fiber, as mentioned in Chapter 6. The fiber is squeezed either by an electromagnet or piezoelectro mechanical transducers, as shown in Fig. 12.17a.

The heat-induced polarization controller in Fig. 12.17b uses the temperature dependence of a short length of the birefringence of a polarization-maintaining fiber [26]. The polarization-maintaining fiber, as discussed in Chapter 11, is made of two types of glass having different amounts of shrinkage at the time the glass fiber is set. The birefringence is zero at the temperature T_s when the glass is set. As the temperature T is decreased, the birefringence linearly increases [26] and

$$\beta_b = \alpha \Delta T \tag{12.42}$$

where

$$\Delta T = T_s - T$$

Thus, by changing the temperature, the birefringence can be controlled.

Another type of element is based on the electrooptic effect of an electrooptic [27,28] crystal. The birefringence is varied by an externally applied electric field. An example of an optical guide on a lithium niobate substrate is shown in Fig. 12.17c. The potential V_x between the center and both side electrodes controls the E_x field (vertical field),

and the potential V_y between the two side electrodes controls the E_y field (horizontal field). The proper combination of V_x and V_y provides the required birefringence.

In Fig. 12.17d, a couple of electrically rotatable waveplates are used to convert elliptically polarized input light into linearly polarized light [29]. Light of an arbitrary elliptical polarization can be converted by aligning the fast axis of the quarter-waveplate with either the major or minor axis of the polarization ellipse. The half-waveplate rotates the linearly polarized light to the desired polarization direction (See Section 6.4).

The electrically rotatable waveplates make use of the birefringence of a nematic liquid crystal. The director of the liquid crystal, which behaves like the crystal axis, can be rotated by rotating the external electric field (See Section 5.10.4.2).

12.9.1.2 Polarization Diversity Method

Figure 12.18 shows a block diagram of an example of the polarization diversity method [30,31]. Incident light of an arbitrary polarization state is first fed through a non polarizing beam splitter (NPBS) and then is decomposed into horizontally and vertically polarized waves by means of a polarizing beamsplitter (PBS). The local oscillator light is coupled through the NPBS and is decomposed into horizontally and vertically polarized waves by being fed into the PBS with its direction of polarization at an angle of 45° to the horizontal direction. The horizontally polarized waves of both the signal and the local oscillator are fed to mixer M_H while the vertically polarized waves are fed into mixer M_V. The output current from the mixer is the IF signal current. Each IF current is then squared by a square operator. The outputs from the square operators are summed to obtain the sum of the squares of the horizontal and vertical components. This sum is independent of the state of polarization of the input signal, as proved below.

Any state of polarization can be designated by two parameters. One is the phase difference α between the vertical and horizontal waves, and the other is the power fraction β between the two waves. Both α and β are subject to fluctuations during transmission. The polarization diversity method eliminates both α and β from the final

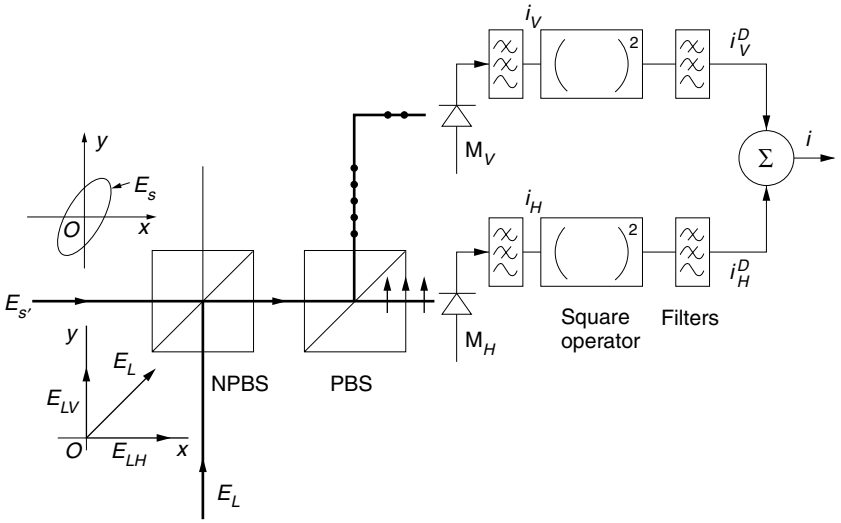

Figure 12.18 Block diagram of the polarization diversity method.

expression. The horizontally and vertically polarized signal and local oscillator fields are represented by

$$\left.\begin{aligned} E_H &= \sqrt{\beta}S(t)\cos\omega_c t \\ E_V &= \sqrt{(1-\beta)}S(t)\cos(\omega_c t+\alpha) \end{aligned}\right\} \tag{12.43}$$

$$E_{LH} = E_{LV} = \frac{1}{\sqrt{2}}E_{\mathrm{LO}}\cos\omega_L t \tag{12.44}$$

The outputs from mixers M_H and M_V are

$$i_H = 2K\left\langle\left(\sqrt{\beta}S(t)\cos\omega_c t + \frac{E_{\mathrm{LO}}}{\sqrt{2}}\cos\omega_L t\right)^2\right\rangle \tag{12.45}$$

$$i_V = 2K\left\langle\left(\sqrt{1-\beta}S(t)\cos(\omega_c t+\alpha) + \frac{E_{\mathrm{LO}}}{\sqrt{2}}\cos\omega_L t\right)^2\right\rangle \tag{12.46}$$

After time averaging and filtering the signal currents from M_H and M_V, the IF frequency components become

$$i_H = \sqrt{2}K\sqrt{\beta}S(t)E_{\mathrm{LO}}\cos\omega_{\mathrm{IF}}t \tag{12.47}$$

$$i_V = \sqrt{2}K\sqrt{1-\beta}S(t)E_{\mathrm{LO}}\cos(\omega_{\mathrm{IF}}t+\alpha) \tag{12.48}$$

The outputs from the square operator after low-pass filtering are

$$i_H^D = [KE_{\mathrm{LO}}S(t)]^2\beta \tag{12.49}$$

$$i_V^D = [KE_{\mathrm{LO}}S(t)]^2(1-\beta) \tag{12.50}$$

It is good to remember that the square operator followed by low-pass filtering always removes the effect of carrier phase fluctuation. Finally, the sum of i_H^D and i_V^D gives

$$i = [KE_{\mathrm{LO}}S(t)]^2 \tag{12.51}$$

which is completely independent of fluctuations in both α and β.

12.9.2 Phase Jitter

Besides polarization jitter, the other jitter to be concerned about is phase jitter, which is generated not only in the laser diode but also in the fiber due to temperature fluctuations and mechanical vibrations. For the amplitude or intensity modulated signal, the modulation information is extracted from only the amplitude of the signal, and the phase jitter does not show up in the output.

Phase jitter in the phase modulated system, however, is more difficult to remove, simply because the system has to identify the origin of the phase change and find out if it is due to the intended phase change associated with the phase modulation, or due to unwanted phase jitter of the system. The two-frequency method is one of the ways to remove the phase jitter and still retain the modulated phase information. The transmitter

sends two light signals whose carrier frequencies are slightly different [31]. Only one lightwave is phase modulated. The frequency of the other unmodulated lightwave is shifted by a small amount $\Delta\omega$. The unmodulated light is a tone signal used as reference. The two light signals are transmitted through the same fiber, at the same time, under the same conditions, and at the same state of polarization, and it is reasonable to expect that both suffer the same phase jitter during transmission. If the two phases are subtracted from each other at the receiver, only the intended phase modulation will be detected.

First, it is assumed that the polarization jitter is absent. Figure 12.19 shows the circuit of a differential phase shift keying (DPSK) system. The transmitter laser lightwave is divided into two lightwaves. One is phase modulated as $\Phi(t)$, and the other is the frequency-shifted tone $\omega_c + \Delta\omega$. In this example, the frequency shift $\Delta\omega$ is created by an acoustooptic modulator. Prior to entering the fiber-optic cable, both waves are combined such that the two waves are polarized in the same direction. At the receiver end, both waves are mixed with the local oscillator and undergo detection and signal processing. Both waves emerging from the fiber will have undergone similar phase and polarization jitter. A fiber-loop polarization controller [22] (FPC) is used to convert the waves back to a linear polarization. Then, the waves are mixed with the local oscillator through a nonpolarizing beamsplitter (NPBS). Let α denote the phase jitter from the fiber during transmission. The output from the mixer M is

$$i = 2K\langle\{\cos[\omega_c t + \Phi(t) + \theta + \theta_p + \alpha] + \cos[(\omega_c + \Delta\omega)t + \theta + \alpha] + E_{\mathrm{LO}}\cos(\omega_L t + \theta_L)\}^2\rangle \tag{12.52}$$

where θ, θ_p, and θ_L are the phase jitters in the transmitter laser, the phase modulator, and the local oscillator laser, respectively. For simplicity, the wave amplitude $S(t)$ has been taken as unity.

The output is band-pass filtered so that the $\Delta\omega$ component is rejected. Only the ω_{IF} and $(\omega_{\mathrm{IF}} + \Delta\omega)$ components are retained, where $2\omega_c$, $2\omega_L$, and $(\omega_c + \omega_L)$ terms are ignored.

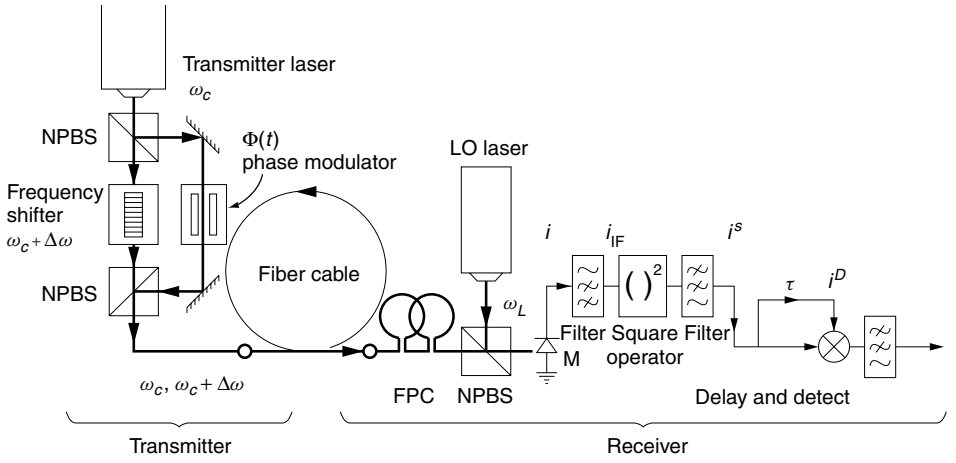

Figure 12.19 Phase jitter removal from a DPSK system by a frequency shift delay- and-detect method.

The output current from the filter is

$$\begin{aligned} i_{\mathrm{IF}} = 2KE_{\mathrm{LO}}\{&\cos(\omega_{\mathrm{IF}}t + \Phi(t) + \theta - \theta_L + \theta_p + \alpha] \\ &+ \cos[(\omega_{\mathrm{IF}} + \Delta\omega)t + \theta - \theta_L + \alpha]\} \end{aligned} \tag{12.53}$$

After the square operator, the term with $\Delta\omega$ is selected by filtering. The ac output is

$$i^s = 4(KE_{\mathrm{LO}})^2 \cos[\Delta\omega t - \Phi(t) - \theta_p] \tag{12.54}$$

Equation (12.54) contains the desired phase modulation information $\Phi(t)$ and is free from fluctuations in θ, θ_L, and α. However, the phase jitter term from the phase modulator itself is still present.

DPSK is the coding system that uses the change in the phase of the carrier. A "0" is represented by the absence of change; a "1" is represented by the presence of change. The means by which the delay-and-detect circuit interrogates the DPSK coding will be explained. Besides the function of interrogation, the delay-and-detect circuit also removes the θ_p noise. The signal path of the delay-and-detect circuit is divided into two paths, one having a shorter length than the other. The output from the longer path is time delayed from that of the shorter path by exactly one bit period. The sum of these two signals are squared, and all the terms except the product of these two signals are filtered out. The result is

$$i^D = K_1 \cos[\Delta\omega(t - \tau) - \Phi(t - \tau) - \theta_p] \cos[\Delta\omega t - \Phi(t) - \theta_p] \tag{12.55}$$

where K_1 absorbs all the physical parameters, and τ is one bit period. The output is fed through a low-pass filter and

$$i^D = \tfrac{1}{2}K_1 \cos[\Delta\omega\tau + \Phi(t - \tau) - \Phi(t)] \tag{12.56}$$

Imposing the condition that

$$\Delta\omega\tau = 2N\pi, \quad \text{where } N \text{ is an integer} \tag{12.57}$$

the "0" bit and the "1" bit of the phase modulation satisfy

$$\begin{aligned} \Phi(t - \tau) &= \Phi(t) && \text{"0" bit} \\ \Phi(t - \tau) &= \Phi(t) + \pi && \text{"1" bit} \end{aligned} \tag{12.58}$$

Thus, the output from the detector becomes

$$i^D = \begin{cases} K/2 & \text{for "0" bit} \\ -K/2 & \text{for "1" bit} \end{cases} \tag{12.59}$$

Therefore, all the phase jitter is removed from the detected signal. The signs of $K/2$ in Eq. (12.59) are reversed if $2N$ in Eq. (12.57) is replaced by $2N + 1$.

It may be added that even though the delay-and-detect circuit has the merit of simplicity, there is a restriction on the choice of the bit rate, as specified by Eq. (12.57). Equation (12.57) can be rewritten in terms of the bit rate $B = 1/\tau$ as

$$B = \frac{\Delta f}{N} \tag{12.60}$$

where $\Delta f = \Delta\omega/2\pi$ and $N = 1, 2, 3\ldots$. The delay-and-detect circuit cannot function (See Problem 12.3) when

$$B = \frac{4}{(2N-1)}\Delta f \tag{12.61}$$

where $N = 0, 1, 2, 3\ldots$.

12.10 COHERENT DETECTION IMMUNE TO BOTH POLARIZATION AND PHASE JITTER

Two systems that are free from both polarization and phase jitter will be presented here. Both systems combine a circuit designed to eliminate phase jitter with a circuit designed to get rid of polarization jitter, but they combine them in different ways. The first example uses the two diversities separately while the second example uses the two diversities in a more comprehensive manner.

Figure 12.20 shows a block diagram of the first example [32]. Phase diversity is applied to the horizontal and vertical waves separately and polarization diversity

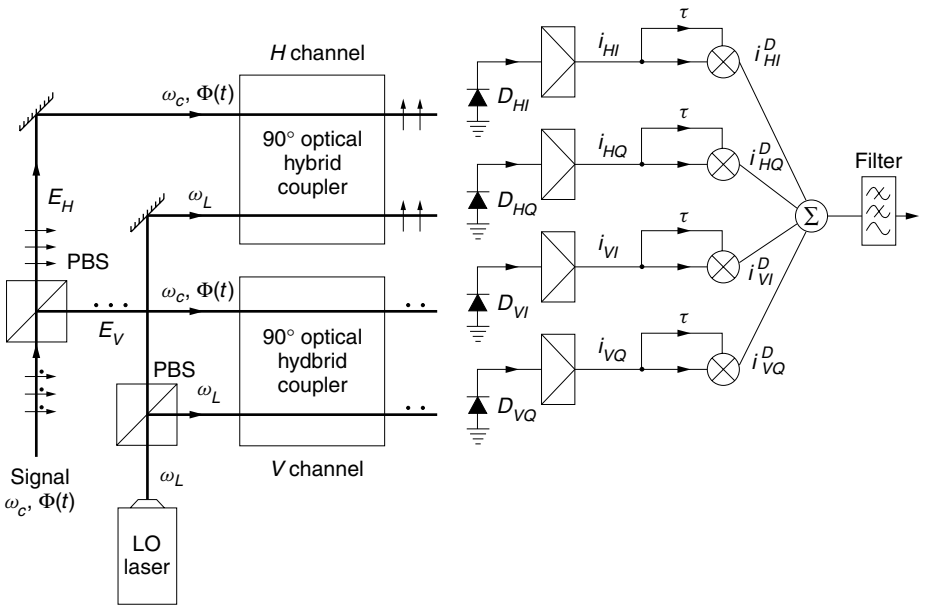

Figure 12.20 Block diagram of DPSK that is free from both polarization and phase jitter. (After Y. H. Cheng, T. Okoshi, and O. Ishida [32].)

is applied to these two phase-jitter-free waves. This example again uses DPSK modulation. The received signal is first fed to the polarization beamsplitter. The horizontal and vertical wave outputs from the beamsplitter are

$$E_H = \sqrt{\beta} S(t) \cos[\omega_c t + \Phi(t) + \theta_H] \tag{12.62}$$

$$E_V = \sqrt{1-\beta} S(t) \cos[\omega_c t + \Phi(t) + \theta_V] \tag{12.63}$$

where the fluctuating quantities are β, θ_H, and θ_V. They are fed to separate 90° optical hybrid couplers together with the local oscillator light. The output from the 90° optical hybrid is similar to the one in Fig. 12.9 described in connection with the optical Costas loop in Section 12.6.2. The in-phase and quadrature phase IF frequency outputs for the horizontal wave components are

$$i_{HI} = \sqrt{2} K \sqrt{\beta} E_{\text{LO}} S(t) \cos[\omega_{\text{IF}} t + \Phi(t) + \theta_H] \tag{12.64}$$

$$i_{HQ} = \sqrt{2} K \sqrt{\beta} E_{\text{LO}} S(t) \sin[\omega_{\text{IF}} + \Phi(t) + \theta_H] \tag{12.65}$$

where the local oscillator power is equally divided into each 90° hybrid coupler and its amplitude is $(1/\sqrt{2})E_{\text{LO}}$.

Similarly, the outputs from the 90° hybrid coupler for the vertical wave components are

$$i_{VI} = \sqrt{2} K \sqrt{(1-\beta)} E_{\text{LO}} S(t) \cos[\omega_{\text{IF}} t + \Phi(t) + \theta_V] \tag{12.66}$$

$$i_{VQ} = \sqrt{2} K \sqrt{(1-\beta)} E_{\text{LO}} S(t) \sin[\omega_{\text{IF}} t + \Phi(t) + \theta_V] \tag{12.67}$$

These IF signals are separately amplified and then fed to sets of delay-and-detect circuits. The delay-and-detect circuit performs the operation of the product between the present and previous bits, as described in Section 12.9.2.

Now let us obtain the horizontal wave output from the top delay-and-detect circuits. Note that the delay-and-detect circuit in Fig. 12.20 does not employ a low-pass filter as compared to that in Fig. 12.19. The output for the in-phase component is the product of i_{HI} at $t = t$ and $t = t - \tau$ with $\Phi(t - \tau) = \Phi(\tau)$ for "0" and $\Phi(t - \tau) = \Phi(t) + \pi$ for "1".

$$i_{HI}^D = \pm \beta K_m [K E_{\text{LO}} S(t)]^2 \cos^2[\omega_{\text{IF}} t + \Phi(t) + \theta_H] \tag{12.68}$$

where the + sign corresponds to the "0" bit and the − sign to the "1" bit, and where K_m is a constant associated with the electronic mixer and $\omega_{\text{IF}} \tau = 2N\pi$. Similarly, the output for the quadrature phase component is

$$i_{HQ}^D = \pm \beta K_m [K E_{\text{LO}} S(t)]^2 \sin^2[\omega_{\text{IF}} t + \Phi(t) + \theta_H] \tag{12.69}$$

The sum of Eqs. (12.68) and (12.69) is independent of ω_{IF}, $\Phi(t)$, and θ_H.

$$i_H = \pm \beta K_m [K E_{\text{LO}} S(t)]^2 \tag{12.70}$$

The components for the vertically polarized waves are

$$i_{VI}^{D} = \pm(1-\beta)K_m[KE_{\mathrm{LO}}S(t)]^2\cos^2[\omega_{\mathrm{IF}}t + \Phi(t) + \theta_V] \tag{12.71}$$

$$i_{VQ}^{D} = \pm(1-\beta)K_m[KE_{\mathrm{LO}}S(t)]^2\sin^2[\omega_{\mathrm{IF}}t + \Phi(t) + \theta_V] \tag{12.72}$$

Addition of Eqs. (12.71) and (12.72) gives

$$i_V = \pm(1-\beta)K_m[KE_{\mathrm{LO}}S(t)]^2 \tag{12.73}$$

Finally, the sum of Eqs. (12.70) and (12.73) removes the fluctuation of β in polarization, and gives a completely jitter-free signal:

$$i = \pm K_m[KE_{\mathrm{LO}}S(t)]^2 \tag{12.74}$$

The system with the square operation that also achieves jitter-free operation for DPSK modulation is shown in Fig. 12.21. This system combines the two diversity methods more comprehensively [33]. This system uses the frequency shift method for phase jitter cancellation, and the square and addition operation for polarization diversity. This system is simpler than the previous system in that both the unshifted signal and the frequency-shifted signal share the same circuit, but it requires a frequency-shifted signal light. The transmitting light consists of two waves. One is at frequency ω_c and is phase modulated by $\Phi(t)$ of the DPSK data. The other is frequency shifted to $\omega_c + \Delta\omega$ but is not modulated. Both of these waves are linearly polarized and the directions of polarization of the two waves are collinear.

Just the same as the system in Fig. 12.19, during the traversal of the fiber, both waves experience the same phase jitter and change of state of polarization because the

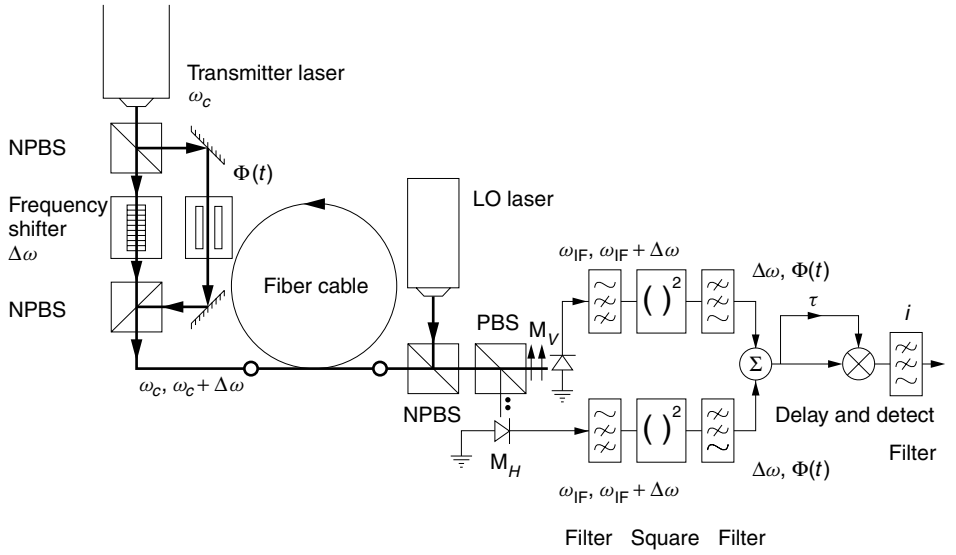

Figure 12.21 System with the square operation for the removal of both polarization and phase jitter from DPSK.

only difference between the two waves is that one is frequency shifted by $\Delta\omega$. The received signals become

$$E_H = \frac{1}{\sqrt{2}}\sqrt{\beta}S(t)\{\cos[\omega_c t + \Phi(t) + \theta + \theta_p + \theta_H] + \cos[(\omega_c + \Delta\omega)t + \theta + \theta_H]\} \tag{12.75}$$

$$E_V = \frac{1}{\sqrt{2}}\sqrt{1-\beta}S(t)\{\cos[\omega_c t + \Phi(t) + \theta_p + \theta_V] + \cos[(\omega_c + \Delta\omega)t + \theta + \theta_V]\} \tag{12.76}$$

where θ_p is the jitter in the phase modulator and θ, θ_H, and θ_V are the same as before and are the phase jitters of the source, the horizontal wave, and the vertical wave. The received wave is separated into horizontal and vertical wave channels. The local oscillator signal is

$$E_L = E_{\text{LO}} \cos(\omega_L t + \theta_L) \tag{12.77}$$

which is polarized at 45° to the horizontal direction, providing an equal-amplitude ($E_{\text{LO}}/\sqrt{2}$) local oscillator field to each channel, where E_{LO}, ω_L, and θ_L are the local oscillator amplitude, frequency, and phase jitter. The analysis of the operation is quite similar to that of the phase diversity without polarization diversity described in Section 12.9.1.2 and will be repeated only briefly. In each channel, the signal is converted down to the IF frequency by the mixers M_H and M_V. In each channel, a band-pass filter follows the mixer and filters out the $\Delta\omega$ component, keeping only ω_{IF} and $\omega_{\text{IF}} + \Delta\omega$ components. These two components experience the same phase jitter, and the next processing step consisting of the square operation followed by summation serves to cancel the phase jitter. Thus, signals in both the H and V channels become free from phase jitter. Using results similar to Eq. (12.53) as the input to the square operator, the squared results of the H and V channels are

$$i_H = 2[KE_{\text{LO}}S(t)]^2\beta\cos[\Delta\omega t - \Phi(t) - \theta_p] \tag{12.78}$$

$$i_V = 2[KE_{\text{LO}}S(t)]^2(1-\beta)\cos[\Delta\omega t - \Phi(t) - \theta_p] \tag{12.79}$$

Addition of the two outputs becomes independent of fluctuating β and

$$i = 2[KE_{\text{LO}}S(t)]^2\cos[\Delta\omega t - \Phi(t) - \theta_p] \tag{12.80}$$

Finally, the signal from the delay-and-detect of Eq. (12.80), followed by a low-pass filter, becomes

$$i = \frac{K_1}{2}\cos[\Delta\omega\tau + \Phi(t-\tau) - \Phi(t)] \tag{12.81}$$

where K_1 absorbs all the physical parameters. The output is completely free from both phase and polarization jitter. An advantage of this system over the previous system is that the lightwaves of ω_c and $\omega_c + \Delta\omega$ share the same paths, and the receiving system is simpler in this regard. The disadvantage is the requirement of a more elaborate transmitting system.

The existing PBS in Fig. 12.21 cannot be used to mix the local oscillator beam with the signal beam, thereby sparing a NPBS, because the direction of the polarizations of the emergent signal and the local oscillator beams become perpendicular to each other.

12.11 CONCLUDING REMARKS

At the receiving end, the transmitted light signal is converted back into the original encoded electrical signal. Receiving systems can broadly be categorized into the following five systems:

1. Direct detection (or video detection).
2. Heterodyne detection.
3. Homodyne detection.
4. Intradyne detection.
5. Detection by stimulated effects.

The advantages and disadvantages of these systems are summarized below.

1. The direct detection scheme is simple, but the trade-off for simplicity is mediocre sensitivity and the lack of a built-in mechanism for channel selectivity. With direct detection, channel selectivity is achieved with additional components such as wavelength filters. Even when such filters are used, channel selectivity is generally poorer than what can be achieved with heterodyne and homodyne detection.
2. The heterodyne system is equipped with a local oscillator laser and is therefore more complicated than direct detection, but it enjoys more than a 20-dB improvement in receiver sensitivity as well as more than 10^3 times the wavelength selectivity.
3. The homodyne system is similar to the heterodyne system but with zero intermediate frequency (IF). With zero IF, the frequency bandwidth per channel is smaller, and the receiver gain is 3 dB higher, compared to a heterodyne system. The price to be paid is that the homodyne system requires a local oscillator laser that can track the phase of the signal wave, and this requirement is very severe.
4. Intradyne detection is a mixture of heterodyne and homodyne detection systems. The stability requirement of the local oscillator is not as severe as that of the homodyne detection.
5. The stimulated effect uses stimulated Brillouin scattering and the system can be interpreted as detection with built-in phase tracking. The narrowness of the frequency bandwidth and difficulty in applying ASK modulation are disadvantages of this system.

PROBLEMS

12.1 (a) What is the theoretical limit ($\eta = 1$) for the output current from a PIN photodiode when the power of the incident light is -43 dBm and the wavelength is $\lambda = 0.84$ μm?

(b) What value was assigned to the quantum efficiency to obtain the rule of thumb equation $i = 0.5$ A/W for expressing the output current i from a PIN photodiode?

12.2 With the polarization diversified circuit shown in Fig. 12.18, prove that as long as the ASK format is used, the phase jitter incurred in both the transmitting and local oscillator lasers, as well as in the fiber during transmission, can be removed.

12.3 Prove that the delay-and-detect circuit cannot function when the bit rate B is

$$B = \frac{4}{2N-1}\Delta f$$

where Δf is the frequency shift between the two frequencies of the double-frequency scheme mentioned in Section 12.9.2.

REFERENCES

1. Y. Tsuchiya, "Streak cameras for ultrafast time resolved photon detection," *Proc. SPIE* **1599**, 244–270 (1991).
2. C. Kittel, *Introduction to Solid State Physics*, 7th ed., Wiley, New York, 1996.
3. B. Sapoval and C. Herman, *Physics of Semiconductors*, Springer-Verlag, Berlin, 1995.
4. H. Yonezu, *Engineering of Components of Fiber Optic Communication*, 2nd ed. (in Japanese), Kogakutosho, Tokyo, 1986.
5. F. Zappa, A. Lacaita, S. Cova, and P. Lovati, "Counting, timing, and tracking with a single-photon germanium detector," *Opt. Lett.* **21**(1), 59–61 (1996).
6. S. Ryu, *Coherent Lightwave Communication Systems*, Artech House, Boston, 1995.
7. T. Okoshi, "Recent advances in coherent optical fiber communication systems," *J. Lightwave Technol.* **5**(1), 44–52 (1987).
8. L. G. Kazovsky, S. Benedetto, and A. Willner, *Optical Fiber Communication Systems*, Artech House, Boston, 1996.
9. M. A. Grant, W. C. Michie, and M. J. Fletcher, "The performance of optical phase-locked loops in the presence of nonnegligible loop propagation delay," *J. Lightwave Technol.*, **5**(4), 592–597 (1987).
10. A. W. Davis, M. J. Pettitt, J. P. King, and S. Wright, "Phase diversity techniques for coherent optical receivers," *J. Lightwave Technol.* **5**(4), 561–572 (1987).
11. G. Nicholson and T. D. Stephens, "Performance analysis of coherent optical phase diversity receivers with DPSK modulation," *J. Lightwave Technol.* **7**(2), 393–399 (1989).
12. I. B. Djordjević, M. C. Stefanović, S. S. Ilić, and G. T. Djordjević, "An example of a hybrid system: Coherent optical system with Costas loop in receiver-system for transmission in baseband," *J. Lightwave Technol.* **16**(2), 177–183 (1998).
13. G. L. Abbas, V. W. S. Chan, and T. K. Yee, "A dual-detector optical heterodyne receiver for local oscillator noise suppression," *J. Lightwave Technol.* **3**(5), 1110–1122 (1985).
14. D. Cotter, "Stimulated Brillouin scattering in monomode optical fiber," *J. Opt. Commun.* **4**, 10–19 (1983).
15. Y. -H. Lee, H. -W. Tsao, M. -S. Kao, and J. Wu, "Application of fiber Brillouin amplifiers on coherent optical wavelength division and subcarrier-multiplexing (WDM-SCM) system," *J. Opt. Commun.* **13**(3), 99–103 (1992).

16. S. Fischer, P. Meyrueis, and W. Schroder, "Brillouin backscattering in fiber optic gyroscope," *Proc. SPIE* **2510**, 49–58 (1995).
17. G. P. Agrawal, *Fiber-Optic Communication Systems*, 2nd ed., Wiley, New York, 1997.
18. U. L. Österberg, "Nonlinear optics: Theory and applications," *Trends in Optical Fibre Metrology and Standards*, edited by O. D. D. Soares, *Proceedings of the NATO Advanced Study Institute*, **285**, Viana do Castelo, Portugal, pp. 711–725, 1994.
19. E. M. Dianov, M. V. Grekov, L. A. Bufetov, S. A. Vasiliev, O. I. Medvedkov, G. A. Ivanov, A. V. Belov, V. G. Plotnichenko, V. V. Koltashev, and A. M. Prokhorov, "Phosphosilicate fiber: Simple high-power CW 1.24 and 1.48 μm Raman lasers," *CLEO'98*, San Francisco, p. 225, May 3–8, 1998.
20. J. -L. Archambault and S. G. Grubb, "Fiber gratings in lasers and amplifiers," *J. Lightwave Technol.* **15**(8), 1378–1390 (1997).
21. R. Ulrich, S. C. Rashleigh, and W. Eickhoff, "Bending-induced birefringence in single-mode fibers," *Opt. Lett.* **5**(6), 273–275 (1980).
22. H. C. Lefevre, "Single-mode fiber fractional wave devices and polarization controllers," *Electron. Lett.* **16**(20), 778–780 (1980).
23. R. A. Harmon, "Polarization stability in long lengths of monomode fibre," *Electron. Lett.* **18**(24), 1058–1059 (1982).
24. I. Andonovic and D. Uttamchandani, *Principles of Modern Optical Systems*, Artech House, Norwood, MA, 1989.
25. A. S. Siddiqui and Y. Aihua, "A new method to analyze the endless characteristics of polarization controllers," *J. Opt. Commun.* **10**(4), 141–143 (1989).
26. N. G. Walker and G. R. Walker, "Survey and current status of polarization control techniques for coherent optical communications," *Proc. SPIE* **1175**, 67–79 (1990).
27. N. G. Walker and G. R. Walker, "Polarization control for coherent communications," *J. Lightwave Technol.* **8**(3), 438–458 (1990).
28. P. T. Fredericksen, M. Flüge, E. Dietrich, and H. G. Weber, "A fast polarization controller for coherent phase diversity receivers," *J. Opt. Commun.* **10**(4), 149–153 (1989).
29. T. Chiba, Y. Ohtera, and S. Kawakami, "Polarization stabilizer using liquid crystal rotatable waveplates," *J. Lightwave Technol.* **17**(5), 885–890 (1999).
30. B. Glance, "Polarization independent coherent optical receiver," *J. Lightwave Technol.* **5**(2), 274–276 (1987).
31. R. T. B. James, K. Iizuka, and Y. Imai, "Phase noise cancelled polarization diversity scheme for DPSK optical communication," *Electron. Lett.* **25**(20), 1394–1396 (Sept. 28, 1989).
32. Y. H. Cheng, T. Okoshi, and O. Ishida, "Performance analysis and experiment of a homodyne receiver insensitive to both polarization and phase fluctuations," *J. Lightwave Technol.* **7**(2), 368–374 (1989).
33. Y. Imai, K. Iizuka, and R. T. B. James, "Phase-noise-free coherent optical communication system utilizing differential polarization shift keying (DpolSK)," *J. Lightwave Technol.* **8**(5), 691–697 (1990).